iScience

CellPress
OPEN ACCESS

Article

SARS-CoV-2 antigen-carrying extracellular vesicles activate T cell responses in a human immunogenicity model

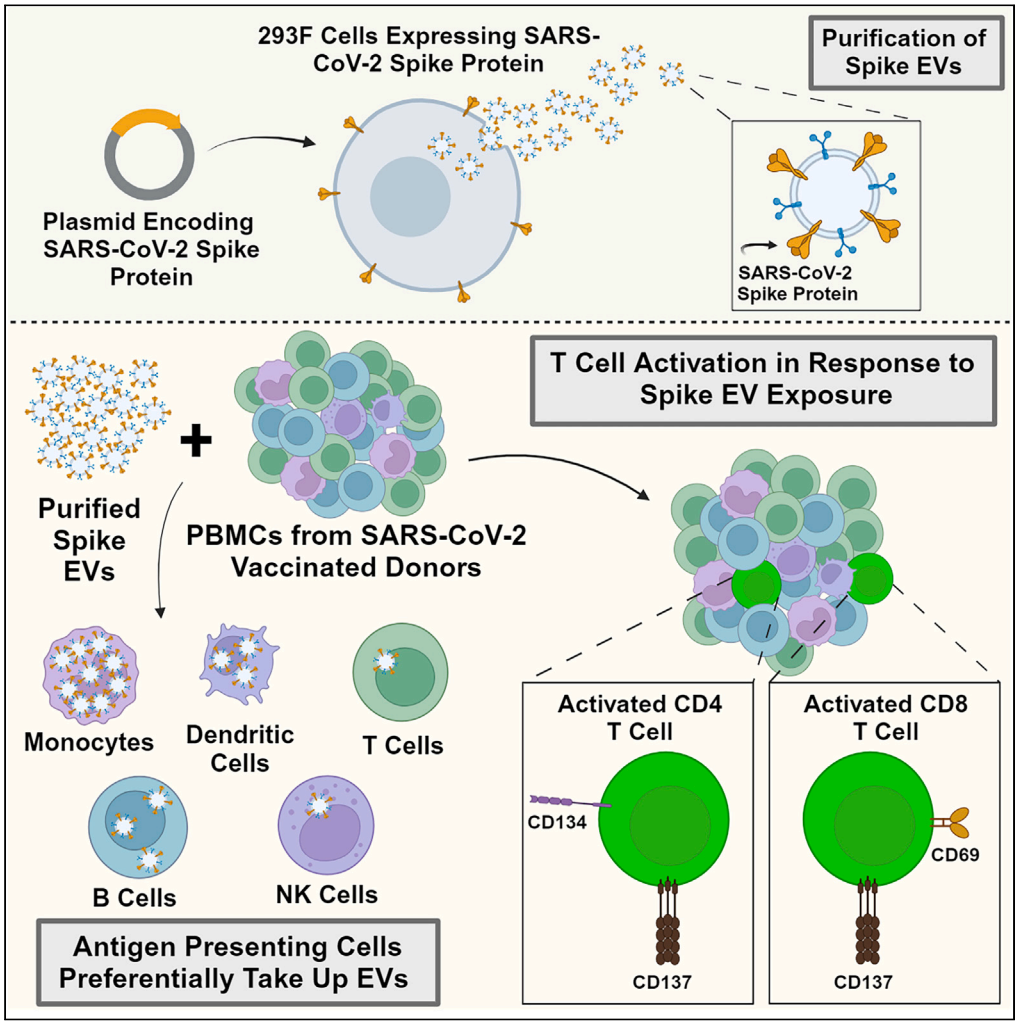

Sarah E. Cummings, Sean P. Delaney, Frederic St-Denis Bissonnette, ..., Tyson E. Graber, Tommy Alain, Jessie R. Lavoie

jessie.lavoie@hc-sc.gc.ca

Highlights

Immunogenicity of antigen-carrying EVs modeled in human cell-based assay

Spike EVs elicit immunogenic responses in T cells while unmodified EVs do not

Spike EVs taken up preferentially by antigen-presenting cells in mixed PBMCS

Human cell-based assay models EV-mediated antigen delivery, uptake and presentation

Cummings et al., iScience 27, 108708
January 19, 2024 Crown

https://doi.org/10.1016/j.isci.2023.108708

iScience

CellPress
OPEN ACCESS

Article

SARS-CoV-2 antigen-carrying extracellular vesicles activate T cell responses in a human immunogenicity model

Sarah E. Cummings,[1,2] Sean P. Delaney,[1,2] Frederic St-Denis Bissonnette,[1,2] Andrew Stalker,[1] Gauri Muradia,[1] Jelica Mehic,[1] Tyson E. Graber,[3] Tommy Alain,[2,3] and Jessie R. Lavoie[1,2,4,*]

SUMMARY

Extracellular vesicles (EVs) are entering the clinical arena as novel biologics for infectious diseases, potentially serving as the immunogenic components of next generation vaccines. However, relevant human assays to evaluate the immunogenicity of EVs carrying viral antigens are lacking, contributing to challenges in translating rodent studies to human clinical trials. Here, we engineered EVs to carry SARS-CoV-2 Spike to evaluate the immunogenicity of antigen-carrying EVs using human peripheral blood mononuclear cells (PBMCs). Delivery of Spike EVs to PBMCs resulted in specific immune cell activation as assessed through T cell activation marker expression. Further, Spike EVs were taken up largely by antigen-presenting cells (monocytes, dendritic cells and B cells). Taken together, this human PBMC-based system models physiologically relevant pathways of antigen delivery, uptake and presentation. In summary, the current study highlights the suitability of using human PBMCs for evaluating the immunogenicity of EVs engineered to carry antigens for infectious disease therapeutics.

INTRODUCTION

Extracellular vesicles (EVs) are nanoscale vesicles that are naturally released by both prokaryotic and eukaryotic cells. The role that EVs play in cell-to-cell communication is essential for many physiological processes and is considered essential for the viability of an organism.[1–4] EVs feature a distinct lipid bilayer and carry molecular signatures, including surface antigens and intravesicular contents, reminiscent of the parent cell from which they are derived.[2,5] Small EVs, defined as vesicles less than 200 nm in diameter, are gaining particular interest in therapeutic applications due in large part to their natural production in biological systems, characteristically nanoscale size and versatility as cargo-carrying vehicles.[6,7] Their size contributes to their versatility as a vehicle as it allows for entry into tissues and typically impenetrable biological barriers, including the blood brain barrier.[8,9] This feature, as well as their capability to package a broad range of cargos, including surface and intravesicular proteins and nucleic acids (DNA and RNA) is propelling these biological vesicles forward into a number of therapeutic applications currently at the clinical stage.

The immunomodulatory potential of EVs, native or engineered, has been a key area of investigation with wide-reaching applications including cancer immunotherapy, regenerative medicine and infectious diseases. For example, native EVs derived from mesenchymal stem/stromal cells (MSCs) have been exploited for their ability to dampen hyperactive immune responses, which may provide therapeutic benefit for inflammatory bowel disease, sepsis and graft-versus-host disease, among others.[10–15] Engineering EVs to generate a tool for modulating the immune system to encourage immunological activity is an alternative strategy gaining traction in the field of cancer immunotherapy. One notable approach currently in late stages of clinical testing is the development of dendritic cell (DC)-derived EVs as cancer vaccines to promote tumor surveillance and cancer cell killing.[16–20]

Growing in popularity is the exploration of EVs as a therapeutic or prophylactic vehicle for infectious diseases. EVs have been investigated as therapeutics in relation to SARS-CoV-2, with a focus on exploiting the immunosuppressive capacity of MSC-derived EVs to dampen the hyperactivity of the immune system while fighting natural infection.[21,22] Additionally, EVs engineered to express ACE2, the cognate receptor for SARS-CoV-2 Spike protein, have been explored as decoy agents to saturate binding domains of viral particles thus preventing infection from taking hold.[23–26] This is further supported by the finding that EVs derived from cell lines naturally expressing high levels of ACE2 were capable of binding multiple Spike proteins simultaneously, while EVs derived from cell lines with negligible ACE2 expression could not.[27] In addition, EVs carrying SARS-CoV-2 Spike protein have been explored as a tool to visualize the binding of anti-Spike neutralizing antibodies

[1]Centre for Oncology, Radiopharmaceuticals and Research, Biologic and Radiopharmaceutical Drugs Directorate, Health Products and Food Branch, Health Canada, Ottawa, ON, Canada
[2]Department of Biochemistry, Microbiology and Immunology, Faculty of Medicine, University of Ottawa, 451 Smyth Road, Ottawa, ON K1H 8M5, Canada
[3]Children's Hospital of Eastern Ontario Research Institute, Ottawa, 401 Smyth Road, Ottawa, ON K1H 8L1 Canada
[4]Lead contact
*Correspondence: jessie.lavoie@hc-sc.gc.ca
https://doi.org/10.1016/j.isci.2023.108708

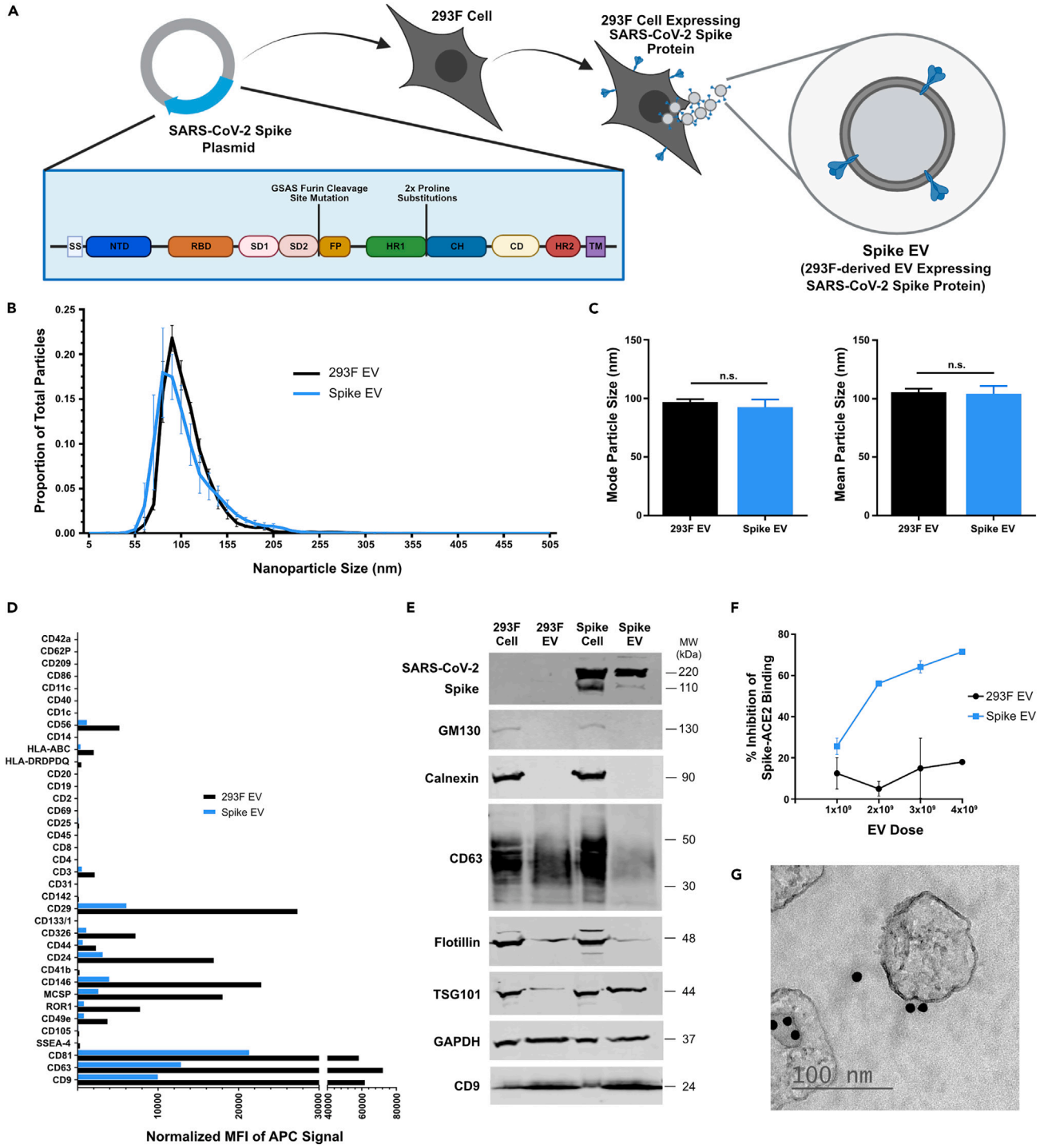

Figure 1. Characterization of 293F cell-derived EVs carrying SARS-CoV-2 spike protein

(A) Schematic of EV engineering strategy using 293F cells including SARS-CoV-2 spike expression construct (see Figure S1) with spike protein depicted in blue. Schematic created with Biorender.com.

(B) Histogram plot of particle size distribution comparing 293F EVs and Spike EVs as determined by NTA. The number of particles falling within each size bin was normalized to total particle counts and are presented as the proportion of total particles. Data represent the mean ± standard error of the mean (SEM). N = 3 independent experiments. Statistical comparisons were carried out by unpaired, two-tailed Student's *t* test where $p < 0.05$ would be considered significant.

Figure 1. *Continued*

(C) Mean and mode particle size of 293F EVs and Spike EVs as determined by NTA. Data represent the mean ± standard error of the mean (SEM). N = 3 independent experiments. Statistical comparisons were carried out by unpaired, two-tailed Student's *t* test where $p < 0.05$ would be considered significant. n.s. indicates not significant.

(D) Multiplexed bead-based profiling assay of 37 surface antigens on 293F EVs and Spike EVs confirming the presence of expected EV surface markers. Data represent the median fluorescent intensity (MFI) of APC signal (reflecting CD63-APC, CD81-APC and CD9-APC counterstaining) following the subtraction of isotype controls. N = 1 independent experiment.

(E) Representative western blots characterizing the presence of SARS-CoV-2 spike protein in Spike EVs and markers known to be present in EV preparations (CD63, CD9, Flotillin, TSG101, GAPDH) as well as the absence of cell contaminant markers (GM130, Calnexin).

(F) Confirmation of SARS-CoV-2 spike protein presence in Spike EVs through competitive Spike-ACE2 binding assay. Spike EVs inhibit the binding of fluorescently labeled, recombinant SARS-CoV-2 spike protein competitively, in a dose-responsive manner, while 293F EVs demonstrate little inhibition. Data are mean ± SEM. N = 2 independent experiments and 2 technical replicates per sample per run.

(G) Transmission electron micrographs of unstained Spike EVs confirming expected EV morphology. SARS-CoV-2 spike protein presence on 293F Spike EVs was also visually confirmed using immunogold labeling where 10 nm gold particles are seen associating with 293F Spike EVs.

with SARS-CoV-2 Spike and to explore the effects of varying environmental conditions on the ability of neutralizing antibodies to bind to SARS-CoV-2 Spike.[28] The exploitation of EVs as a delivery vehicle has also been pursued in the context of SARS-CoV-2 vaccine strategies. Reports of EVs as a vaccine strategy vary widely in terms of the host cell used for EV production (including the use of bacterial-derived outer membrane vesicles) and the choice to use SARS-CoV-2 Spike mRNA or protein in cargo loading.[29–33] In all reports, EVs appear to hold promise as a vehicle of choice to deliver SARS-CoV-2 Spike as an antigen to induce a robust immunogenic response. The ability of EVs to confer an immunogenic response to SARS-CoV-2 Spike protein should perhaps be unsurprising as a report identified circulating EVs containing SARS-CoV-2 Spike protein in the plasma of individuals following vaccination with SARS-CoV-2 mRNA-containing liposomes.[34] Not only were these EVs present, they were suggested to play a role in mediating the immune response mounted against SARS-CoV-2 Spike protein.

Considering the rising interest in EVs as novel vehicles for antigen presentation in infectious diseases such as SARS-CoV-2,[29–32] influenza,[35] respiratory syncytial virus (RSV)[36] and human immunodeficiency virus (HIV),[35,37] it is essential that robust, non-invasive, human model systems are applied to assess their immunogenicity. Currently, the development of EVs as antigen-carrying therapeutics relies heavily on animal modeling, with a lack of methods available to bridge the gap into understanding how immunogenic responses will translate in human systems. It is well known that rodent and human immune systems vary widely, including mechanisms of antigen presentation and relevant activation makers.[38] Thus, there is a need to implement complimentary human-based assays early in the development process to evaluate the safety and efficacy of EVs as antigen-carrying therapeutics in clinical applications. The adoption of such assays early in development will help to facilitate more rapid and less invasive assessments of the product. Further, the mechanism by which EVs accomplish antigen delivery differs from more traditional vaccine candidates. Therefore, while the use of human PBMCs as a surrogate for modeling immune responses is not a novel concept, determining the appropriate adaptations required to successfully apply such an assay to EV biologics or EV-mediated delivery of antigens is needed given the excitement in the clinical sphere surrounding EVs as delivery vehicles. This study employed human-derived peripheral blood mononuclear cells (PBMCs) as an *ex vivo* model to assess the immunogenicity of EVs used as vehicles for the presentation of a viral antigen. Specifically, we have engineered HEK293F-derived EVs to carry the SARS-CoV-2 Spike protein, and after thoroughly characterizing the product, we demonstrate that the immunogenic potential of these EVs can be captured through T cell activation assays using our *ex vivo*, human model system.

RESULTS

SARS-CoV-2 spike extracellular vesicle generation – 293F model system

Using 293F cells as a producer system for EVs, cells were transduced with lentivirus encoding the SARS-CoV-2 Spike protein driven by the EFS-1a promoter (Figure S1). Expression of SARS-CoV-2 Spike protein was first validated in transduced 293F cells (Figure S1). The establishment of this cell line allowed for the continual collection of cell conditioned medium (CCM) used for the purification of EVs (Figures 1A, S1B, and S1C). EVs purified from unmodified 293F cells will simply be denoted 293F EVs, while those derived from SARS-CoV-2 Spike-expressing 293F cells are herein referred to as Spike EVs.

Generated spike extracellular vesicles display characteristic extracellular vesicle identity markers and enrichment of SARS-CoV-2 spike protein

Nanoparticle tracking analysis (NTA) was performed on both 293F EVs and Spike EVs to determine the size distribution profile of each (Figure 1B). The size distribution profile clearly demonstrates that both 293F EVs and Spike EVs fall within the small EV category described in the International Society for Extracellular Vesicles (ISEV) guidelines as EVs ranging from 50 to 200 nm in diameter.[6] Additionally, the size profiles of Spike EVs did not differ from unmodified 293F EVs. This is demonstrated by the determination of the mode and mean particle size (Figure 1C), such that the mode particle size (96.9 nm in diameter for 293F EVs; 92.7 nm for Spike EVs) and mean particle size (105.6 nm in diameter for 293F EVs; 104.3 nm for Spike EVs) did not differ.

Surface marker expression was profiled in 293F EVs and Spike EVs using a multiplex bead-based flow cytometric assay assessing 37 surface antigens. The tetraspanins (CD63, CD81 and CD9) were all highly detectable in both EV populations, although reduced expression of all markers was evident in Spike EVs relative to unmodified 293F EVs (Figure 1D). Additionally, surface antigens characteristic of epithelial cells

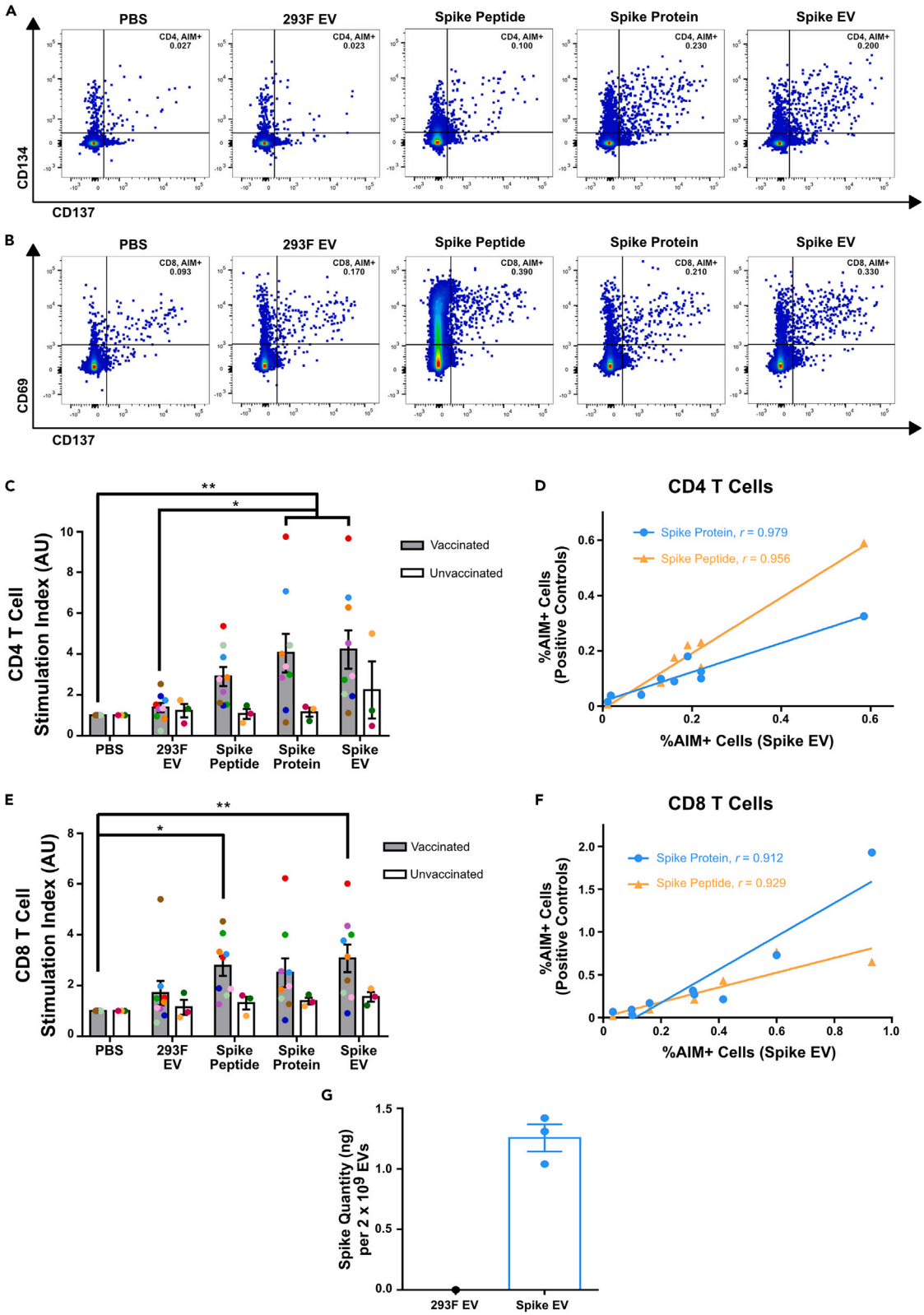
A
PBS
293F EV
Spike Peptide
Spike Protein
Spike EV
CD4, AIM+
0.027
CD4, AIM+
0.023
CD4, AIM+
0.100
CD4, AIM+
0.230
CD4, AIM+
0.200
CD134
CD137
B
PBS
293F EV
Spike Peptide
Spike Protein
Spike EV
CD8, AIM+
0.093
CD8, AIM+
0.170
CD8, AIM+
0.390
CD8, AIM+
0.210
CD8, AIM+
0.330
CD69
CD137
C
CD4 T Cell
Stimulation Index (AU)
Vaccinated
Unvaccinated
PBS
293F EV
Spike Peptide
Spike Protein
Spike EV
D
CD4 T Cells
Spike Protein, r = 0.979
Spike Peptide, r = 0.956
%AIM+ Cells
(Positive Controls)
%AIM+ Cells (Spike EV)
E
CD8 T Cell
Stimulation Index (AU)
Vaccinated
Unvaccinated
PBS
293F EV
Spike Peptide
Spike Protein
Spike EV
F
CD8 T Cells
Spike Protein, r = 0.912
Spike Peptide, r = 0.929
%AIM+ Cells
(Positive Controls)
%AIM+ Cells (Spike EV)
G
Spike Quantity (ng)
per 2 x 10^9 EVs
293F EV
Spike EV

Figure 2. CD4$^+$ and CD8$^+$ T cell Specific Activation in Response to Treatment with Spike EVs

(A) Representative flow cytometric results highlighting activation-induced markers (AIM) (CD134+/CD137+) on CD4$^+$ T cells within PBMCs derived from a single donor (Donor 962) vaccinated against SARS-CoV-2 and stimulated over 48 h with PBS (negative control), SARS-CoV-2 derived peptide covering spike protein (Spike peptide; positive control) or SARS-CoV-2 spike recombinant protein (spike protein; positive control), 293F EVs or Spike EVs. Refer to Figure S2 for full gating strategy.

(B) Representative flow cytometric results highlighting AIM+ (CD69+/CD137+) CD8$^+$ T cells within PBMCs derived from a donor (Donor 962) vaccinated against SARS-CoV-2 and stimulated over 48 h with the same conditions as described in A. Refer to Figure S2 for full gating strategy.

(C) Quantification of CD4$^+$ T cell response measured as percentage of AIM+ (CD134+/CD137+) CD4$^+$ T Cells. Data represent the responses for nine individual vaccinated donors and 3 individual unvaccinated donors (Vaccinated N = 9; Unvaccinated N = 3). Statistical comparisons were carried out by two-way ANOVA with Tukey's multiple comparisons test to compare all treatment groups. *$p < 0.05$; **$p < 0.01$.

(D) Relationship between the frequency of AIM-positive CD4$^+$ T cells in Spike EV treated PBMCs from vaccinated donors and the frequency of AIM-positive CD4$^+$ T cells in the Spike Protein (orange) or Spike Peptide (blue) treatment conditions. N = 9. Pearson's correlation coefficient was computed for the Spike EV and Spike Protein relationship ($r = 0.979$, $p < 0.0001$) and the Spike EV and Spike peptide relationship ($r = 0.956$, $p < 0.0001$).

(E) Quantification of CD8$^+$ T cell response measured as percentage of AIM+ (CD69+/CD137+) CD8$^+$ T Cells. Data represent the responses for nine individual vaccinated donors and 3 individual unvaccinated donors (Vaccinated N = 9, Unvaccinated N = 3). Statistical comparisons were carried out by two-way ANOVA with Tukey's multiple comparisons test to compare all treatment groups. *$p < 0.05$; **$p < 0.01$. E) Relationship between the frequency of AIM-positive CD4$^+$ T cells in Spike EV treated PBMCs from vaccinated donors and the frequency of AIM-positive CD4$^+$ T cells in the Spike Protein (orange) or Spike Peptide (blue) treatment conditions. N = 9. Pearson's correlation coefficient was computed for the Spike EV and Spike Protein relationship ($r = 0.979$, $p < 0.0001$) and the Spike EV and Spike peptide relationship ($r = 0.956$, $p < 0.0001$).

(F) Relationship between the frequency of AIM-positive CD8$^+$ T cells in Spike EV treated PBMCs from vaccinated donors and the frequency of AIM-positive CD4$^+$ T cells in the Spike Protein (orange) or Spike Peptide (blue) treatment conditions. N = 9. Pearson's correlation coefficient was computed for the Spike EV and Spike Protein relationship ($r = 0.912$, $p = 0.0006$) and Spike peptide treatment ($r = 0.929$, $p = 0.0003$).

(G) SARS-CoV-2 spike protein levels in 293F EVs and Spike EVs as determined by ELISA. Data represent the quantity of spike protein normalized to 2 x 109 particles. Data are mean ± SEM. N = 1 and N = 3 independent experiments for 293F EVs and Spike EVs, respectively and 3 technical replicates per sample per run.

and thus expected to be found in 293F cells and their EVs were also detected on our 293F EVs and Spike EVs including CD29 and epithelial cell adhesion molecule (EpCAM) (CD326). Spike EVs demonstrated the same pattern of positive marker expression as 293F EVs, albeit with lower expression of all markers detected. 293F EVs and Spike EVs were lysed to assess SARS-CoV-2 Spike protein expression and classical EV protein markers by Western blot (Figure 1E). First, Spike protein is evidently expressed in transduced 293F cells and Spike EVs while remaining absent as expected in unmodified 293F cells and 293F EVs. Markers expected to be present in EVs, including CD63, CD9, Flotillin, TSG101 and GAPDH, were all present in both 293F EV and Spike EV lysates.[6] The lack of GM130 and calnexin in both 293F EVs and Spike EVs is suggestive of EV preparations free from the contamination of cellular components from the 293F EV producer cells.[6]

In addition to confirming the presence of SARS-CoV-2 Spike protein, it was of interest to assess surface presence and functionality of Spike protein given that the construct used to express this protein was designed with a signal peptide and transmembrane domain to facilitate surface expression. To do so, we employed an ACE2 competitive binding assay as Spike RBD binds ACE2 as one of its cognate receptors.[39,40] Spike EVs interfered with the binding of soluble ACE2 protein to plate-bound recombinant Spike protein in a dose-dependent manner, while little binding inhibition was detected with control 293F EVs (Figure 1F). This suggests that at least some of the Spike protein in Spike EVs is present on the EV surface and is capable of binding to soluble ACE2 protein. The presence of surface SARS-CoV-2 Spike protein on the EVs was also confirmed using gold-labelling and TEM. TEM images further validate particle size as determined by NTA and demonstrate that vesicles are smaller than 200 nm in size (Figures 1G and S5).

Assessing immunogenic properties of spike extracellular vesicles in human blood mononuclear cells as a model system for viral-antigen carrying extracellular vesicles

SARS-CoV-2 Spike protein was chosen to assess responsiveness to an EV-presented viral antigen due to the availability of well characterized samples from individuals recently vaccinated against SARS-CoV-2. PBMCs from vaccinated individuals have been documented to recognize and respond to *ex vivo* challenge with SARS-CoV-2 Spike peptides.[41–43] SARS-CoV-2-specific CD4$^+$ and CD8$^+$ T cell responses can be quantified through the utilization of T cell receptor-dependent activation-induced marker (AIM) assays.[41–43] We stimulated PBMCs from nine independent donors who had been previously vaccinated with two doses of a mRNA-based SARS-CoV-2 vaccine (mRNA-1273 or BNT162b2) as well as PBMCs from three unvaccinated donors for comparison. Details on the donors used in these experiments can be found in Table S1. PBMCs from each donor were stimulated with Spike EVs (1×10^4 EV per PBMC) for 48 h. Additionally, PBS and 293F EV treatments were included as negative controls and SARS-CoV-2 Spike peptides and recombinant protein treatments, respectively denoted Spike peptides and Spike protein herein, were included as positive controls.

T cell responses in CD4$^+$ T cells were assessed using the activation markers CD134 and CD137. Stimulation with Spike EVs resulted in a significant increase in AIM-positive (CD134$^+$/CD137$^+$) CD4$^+$ T cells relative to PBS treatment ($p = 0.0033$; Figures 2A and 2C). Donor-to donor response variability to Spike EV exposure is apparent, with some donors demonstrating high T cell activation and others showing very little. Importantly, this variability aligns with the responses to the recombinant Spike protein and Spike peptide treatments, highlighting a natural variation in the capacity for T cell activation within the SARS-CoV-2 vaccinated population. Specifically, a Pearson correlation coefficient was computed to determine that in CD4$^+$ T cells, a strong positive correlation exists between the AIM-positive responses to Spike EV treatment

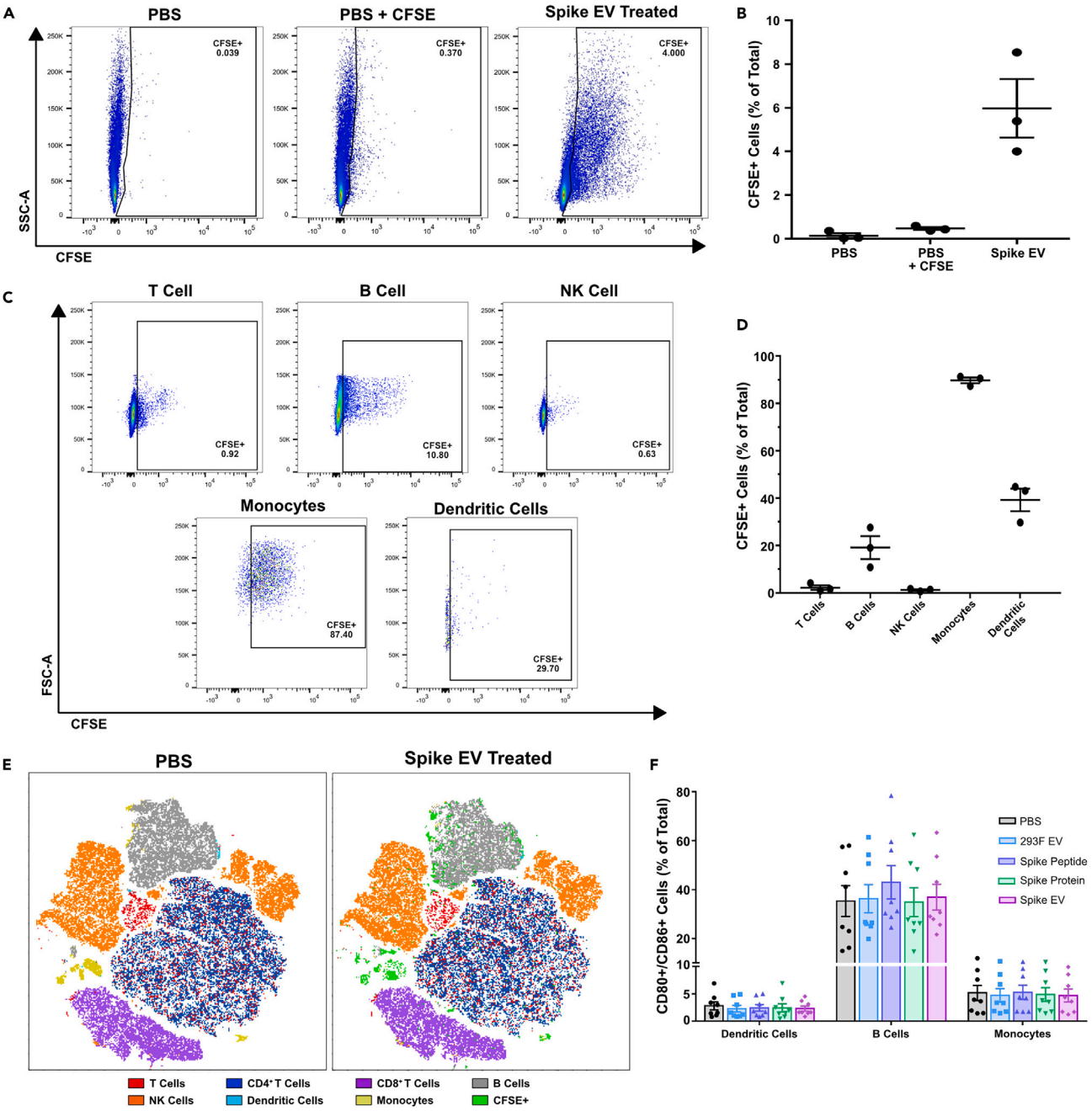

Figure 3. Preferential Uptake of CFSE-Stained Spike EVs in Antigen-Presenting Cells within Mixed Peripheral Blood Mononuclear Cell Population

(A) Representative flow cytometric results of PBMCs derived from a single donor (Donor 965) vaccinated against SARS-CoV-2 and incubated with Spike EVs pre-stained with CFSE as well as PBS only and PBS with CFSE as controls. Flow cytometric plots highlight the frequency of total CFSE-positive cells from a single run following the exclusion of dead cells and doublets (Refer to Figure S3 for gating strategy).

(B) Graphical representation of CFSE signal in PBMCs collected following the conditions outlined in (A). N = 3 independent experiments; Data represent the mean ± SEM.

(C) Representative flow cytometric results of PBMCs following 16 h of incubation with Spike EVs pre-stained with CFSE following manual gating for cell subpopulation analysis. Refer to Figure S3 for full gating strategy.

(D) The percentage of each cell subtype that is CFSE-positive following incubation with CFSE-stained Spike EVs. N = 3 independent experiments; Data represent the mean ± SEM.

(E) t-distributed Stochastic Neighbor Embedding (t-SNE) analysis of live PBMCs after PBS treatment (left plot) or CFSE-stained Spike EV treatment (right plot) to cluster cell subpopulations based on flow cytometric measurements of CD3, CD4, CD8, CD19, CD14, CD16 and HLA-DR. Manual gating of cell populations and CFSE-positivity (fluorescent green) were overlayed to visually depict EV uptake across cell populations.

Figure 3. *Continued*

(F) Percentage of antigen-presenting cells (dendritic cells, B cells and monocytes) displaying the surface expression of CD80 and CD86 as determined by flow cytometry following 24 h stimulation with PBS, SARS-CoV-2 derived peptide pool covering spike protein (Spike peptide) or SARS-CoV-2 spike recombinant protein (Spike protein), 293F EVs or Spike EVs in PBMCs from vaccinated donors. N = 8 independent donors; Data represent the mean ± SEM; Statistical comparisons were carried out by two-way ANOVA with Tukey's multiple comparisons test.

and responses to Spike protein treatment ($r = 0.979$, $p < 0.0001$) and Spike peptide treatment ($r = 0.956$, $p < 0.0001$) (Figure 2D). Notably, treatment with unmodified 293F EVs did not result in an increase in activation markers relative to PBS treatment. Furthermore, neither Spike EV stimulation nor recombinant Spike protein treatment resulted in AIM-positive T cell increases in PBMCs collected from donors unvaccinated against SARS-CoV-2 (Figure 2C).

$CD8^+$ T cell responses were also detected following 48 h of stimulation using an AIM assay. The percent of AIM-positive ($CD69^+/CD137^+$) $CD8^+$ T cells was significantly higher in those stimulated with Spike EVs relative to PBS ($p = 0.0034$), with little to no response detectable in the 293F EV treated condition (Figures 2B and 2E). The activation response of $CD8^+$ T cells to Spike EVs was similar in each donor to the response seen in the positive control treatment condition. Using Pearson correlation coefficients, strong positive correlations were computed in $CD8^+$ T cells between responses to Spike EV treatment and responses to Spike protein treatment ($r = 0.912$, $p = 0.0006$) and Spike peptide treatment ($r = 0.929$, $p = 0.0003$) (Figure 2F). Similar to $CD4^+$ T cells, the frequency of AIM-positive $CD8^+$ T cells were unchanged in PBMCs treated with unmodified 293F EVs. Further in unvaccinated PBMCs, the percentage of AIM-positive $CD8^+$ T cells was unchanged in Spike EV stimulated cells relative to PBS treated controls (Figure 2E).

The amount of SARS-CoV-2 Spike protein in the engineered Spike EVs was quantified using an ELISA designed to detect the receptor binding domain (RBD) of SARS-CoV-2 Spike protein. The mean quantity of Spike protein detected was 1.26 ng in 2×10^9 Spike EVs, which was the EV dose used to treat 2×10^5 PBMCs (Figure 2G). For reference, 1 μg of recombinant Spike protein was used as the positive control in this experiment which yielded similar activation levels to the Spike EV treatment. This suggests that EVs were highly effective at antigen delivery in this human PBMC model system.

Uptake of spike extracellular vesicles by antigen-presenting cells in *ex vivo* vaccinated human blood mononuclear cell cultures

Given the activation response detected in PBMCs following Spike EV treatment we sought to determine whether Spike EVs were being taken up by physiologically relevant cell types within the mixed PBMC population in *ex vivo* conditions. To address this, Spike EVs were fluorescently labeled with CFSE and used to treat PBMCs from a single vaccinated donor (Donor 965). PBS combined with CFSE and washed alongside labeled EVs was used as a negative control. Following 16 h of PBMC-EV co-incubation, cells were analyzed by flow cytometry for cell phenotyping of the mixed PBMC population and tracking of EV uptake using CFSE fluorescence as a surrogate marker. On average, 5.98% of all PBMCs were CFSE-positive following Spike-EV treatment (Figures 3A and 3B). Using phenotypic markers, PBMCs were isolated into specific cell subsets including T cells, B cells, natural killer (NK) cells, DCs and monocytes (Figure S5 for full gating strategy). From this subset analysis, an average of 89.8% of monocytes were CFSE-positive, suggesting that 89.8% of all monocytes in the culture took up EVs. DCs and B cells took up moderate numbers of EVs as represented by 39.2% of all DCs and 19.1% of all B cells demonstrating CFSE-positivity. This is contrasted by the very low percentage of T cells (2.2%) and NK cells (1.25%) that were positive for CFSE (Figures 3C and 3D). Visualizing PBMC cell subtypes through t-distributed stochastic neighbor embedding (t-SNE) clustering of flow cytometric data clearly demonstrates the co-localization of CFSE signal with the monocyte population, as well as B cells and DCs (Figure 3E).

Having demonstrated that cells with antigen presenting capacity were also the cells most able to take up Spike EVs *ex vivo*, we sought to determine whether antigen-presenting cells were specifically activated upon stimulation with Spike EVs, ultimately contributing to the specificity of the T cell response. The activation status of dendritic cells, monocytes and B cells in PBMCs from vaccinated donors were quantified through the surface expression of the costimulatory molecules CD80 and CD86 by flow cytometry. In all three cell types interrogated, the percentage of cells that expressed both CD80 and CD86 on the surface remained stable across all treatment groups (Figure 3F). Although a high degree of variability existed between donors, treatment with 293F EVs, Spike controls and Spike EVs all exhibited similar expression levels to their PBS control counterparts. Additionally, no change in CD80/CD86 expression levels in any of the treatment groups was detected in PBMCs from unvaccinated donors either (data not shown). Taken together, these data suggest that the specificity of the T cell response to Spike EV is mediated by the T cell itself as opposed to specific activation of antigen-presenting cells exposed to the same antigen delivery vehicle.

DISCUSSION

Versatile and well-tolerated nanoparticles are highly sought after to facilitate the delivery of therapeutic cargo for many clinical applications, including infectious diseases. To this end, EVs are being explored as cell-derived, biologically native nanovesicles capable of modulating the immune system and delivering antigens to evoke an immunological response. While the development of EVs as a cancer immunotherapy vaccine dates back much earlier, the first foray into exploiting EVs for the development of a vaccine for infectious diseases was in application to SARS-CoV, published in 2007 by Kuate and colleagues.[44] In this report, EVs were engineered to express SARS-CoV Spike protein fused to the G protein of vesicular stomatitis virus. This report demonstrated promise as inoculated mice produced neutralizing antibodies toward the SARS-CoV virus. Following this report, EVs were further explored as protein vaccine candidates for other infectious diseases including human papilloma virus,[35] HIV,[35,37] influenza[35] and RSV.[36] Finally, with the recent emergence of SARS-CoV-2 and the efforts put toward the swift

development of vaccine candidates, numerous groups have explored the possibility of using EVs either as a prophylactic vaccine for this virus, or as a therapeutic decoy agent. For instance, EVs with the surface expression of the ACE2 receptor show promise as a therapeutic strategy to saturate SARS-CoV-2 virions, interfering with cellular entry and thus preventing or limiting infection.[23–27] As a prophylactic vaccine candidate, Tsai and colleagues demonstrated that the delivery of SARS-CoV-2 Spike mRNA in an EV as a vehicle in animal models was well tolerated and led to robust activation responses including the induction of antigen-reactive $CD4^+$ and $CD8^+$ T cells in splenocytes.[29] A number of groups also sought to develop SARS-CoV-2 protein vaccines using Spike protein as the model antigen and similarly reported robust immunogenic responses in the animal models of choice.[30–33]

Despite the progress made in the field toward the development of EVs as vehicles for antigen presentation, a significant gap remains between preliminary testing of immunogenicity in animal models and an understanding of how this translates to the human immune system. It is well documented that the differences between rodent and human immune systems with regards to antigen presentation and relevant activation markers are numerous.[38] The current study demonstrates the utility of a human-derived PBMC *ex vivo* model that can be easily used to identify immunogenic responses to EVs carrying viral antigens. Using SARS-CoV-2 as a topical infectious disease to study, PBMCs collected from human donors that had been previously vaccinated against the virus with mRNA vaccines generated a measurable activation response overall in both $CD4^+$ and $CD8^+$ T cells when exposed to 293F EVs engineered to express the SARS-CoV-2 spike. Specifically, the *ex vivo* T cell response evoked by EVs carrying a viral antigen involves the upregulation of activation markers known to be physiologically relevant to immunogenicity in humans, including CD137 (4-1BB) and CD134 (OX-40).[45–49] Importantly, these markers remained unchanged in human PBMCs treated with unmodified 293F EVs, suggesting that the T cells in the vaccinated donors are responding specifically to the presentation of Spike as an antigen, and not to the EV in general. Additionally, Spike EV delivery did not elicit the same activation response in PBMCs collected from unvaccinated individuals, further demonstrating the specificity of the response to the presentation of SARS-CoV-2 Spike antigen. However, it must be noted that one unvaccinated donor did demonstrate an increase in AIM-positive $CD4^+$ T cells relative to the other conditions, but did not demonstrate any detectable increase in AIM-positive $CD8^+$ T cells. It is possible that this donor is showing some degree of cross-reactive immunity acquired from a different circulating virus within the *Coronaviridae*. Cross-reactivity to SARS-CoV-2 Spike antigens has been detected and further studied in SARS-CoV-2 unexposed individuals and is largely seen in the $CD4^+$ T cell population with much lower frequencies of cross-reactive responses in $CD8^+$ T cells.[50]

Although PBMCs derived from individuals vaccinated against SARS-CoV-2 demonstrated T cell activation in response to Spike EV delivery overall, it should be noted that a high degree of donor to donor variability was observed in these responses. The inclusion of SARS-CoV-2 Spike peptides and SARS-CoV-2 Spike recombinant protein as controls indicated that the donor to donor variability detected in these assays was not specific to the presentation of Spike by EVs, but rather a variability in the overall responsiveness to SARS-CoV-2 Spike in general. That is, individuals with little to no T cell response to Spike EVs exhibited concomitant low responses to Spike protein control stimulations. This is demonstrated clearly by the correlation analyses conducted on both $CD4^+$ and $CD8^+$ T cells, whereby the frequency of AIM-positive cells exhibit a strong positive correlation between the Spike EV treatment and either the Spike peptide or Spike protein controls. Therefore, this is most suggestive of expected variation in memory responses to SARS-CoV-2 Spike within the population. In future applications, use of this model as a surrogate may be helpful in bridging the transition from animal studies toward human clinical trials with regards to both safety and efficacy linked to immunogenicity; however, donor responses must be qualified with control antigens prior to inclusion in such an assay.

An important component of this human *ex vivo* system is the apparent preservation of expected antigen-cell interactions expected to occur *in vivo*. Previous studies have demonstrated that the extent of EV uptake, as well as uptake mechanisms, are largely recipient cell-specific.[4,51] Within the broad category of immune cells, highly phagocytic cells such as monocytes and dendritic cells, have been shown to take up proportionately more EVs than other cell types.[52–55] Exploration of EV dynamics in our model system revealed that Spike EVs were being taken up by physiologically relevant cell types in the *ex vivo* context, namely monocytes and to a lesser extent B cells and DCs, suggesting that activation responses in T cells were achieved indirectly through neighboring antigen-presenting cells. This finding, using 293F-derived Spike EVs, supports current views in the literature suggesting that EVs have a greater propensity to be taken up by highly phagocytic cells including macrophages and monocytes, or cell lines derived therefrom.[52–55] The bias for EVs to be more readily taken up by these phagocytic cell types may be related to their utility of multiple mechanisms for EV uptake including clathrin-mediated endocytosis, phagocytosis, and lipid raft-mediated endocytosis, although the surface receptors and specific mechanistic pathways involved in the uptake process of antigen-carrying 293F-derived EVs must be more thoroughly characterized.[51,52,56,57] Further, the analysis of EV dynamics within the human PBMC *ex vivo* modeling system presented here has limitations. Namely, characterization of EV uptake dynamics was performed in experimental repeats using a single donor (Donor 965). The extent of donor-to-donor variability in Spike EV uptake remains to be tested.

Within our model system, the bias toward antigen-presenting cell types for EV uptake, as well as the timing for detecting T cell responses, suggests that T cell activation following Spike EV delivery is likely occurring indirectly through antigen-presenting cells. Interestingly, Spike EV treatment did not result in changes to the expression of costimulatory molecules CD80 and CD86 on antigen-presenting cells. However, many studies have highlighted that while the engagement of costimulatory molecules is often required for the development of robust T cell effectors when priming naive T cells, their engagement is redundant during the reactivation of already primed T cells, the latter of which is applicable to the model system presented here.[58–61] Moreover, the consistency of antigen-presenting cell activation across treatment groups demonstrates that the specificity of the T cell responses to Spike proteins and Spike EVs in vaccinated donors is driven by antigen recognition from the T cells, as opposed to a secondary effect driven by the differential activation of antigen-presenting cells following EV treatment.

Utilizing human PBMCs as a surrogate for modeling T cell responses to an antigen of interest is not a novel concept. T cell AIM assays have reliably been used to gain a greater understanding of the involvement of cellular immunity following exposure to, or vaccination against,

certain viruses including SARS-CoV-2.[41,50,62–64] However, adapting this assay for use with EV biologics or EV-mediated delivery of antigens is timely. As EVs continue to be pursued as a new therapeutic modality for infectious diseases, this presents an imminent need for appropriate and effective assays to be established for the evaluation of their functionality and potency. When designing the current study, there was an apparent paucity of reports detailing appropriate conditions for EV-PBMC co-culture for the assessment of immunogenic responses including EV dose, exposure time and activation marker readouts. For example, T cell AIM assays are typically performed with cell collection for flow cytometry occurring a maximum of 24 h post-antigen treatment as this provides an optimal window for detection based on known kinetics of activation marker upregulation when the antigens used are peptides designed for efficient antigen-presentation.[50,62,64] However, adapting this assay for use with EV-mediated antigen delivery required the extension of this timeline to 48 h; this may allow sufficient time for antigen-presenting cells to internalize EVs, process more complex EV-delivered cargoes and present antigens of interest to neighboring T cells which can then begin to upregulate activation marker expression. The current study details a specific method for applying such T cell activation assays to the evaluation of EV biologics to provide optimal immunogenic responses to antigens of interest.

Taken together, this study establishes a versatile, human-applicable immunological model system to address the need for bioassays and methods for evaluating EVs as novel biologics, specifically in the realm of infectious diseases. Further, the application of this method to assess EVs carrying SARS-CoV-2 Spike protein as an antigen of interest supports preliminary reports in the field suggesting that EVs may be suitable, nanoscale carriers of antigen as they were capable of inducing a robust and measurable T cell response in human PBMCs.

Limitations of the study

A primary limitation of the current study is that the modest sample size used does not allow for deeper interrogation of assay efficacy across PBMC donor demographics. It remains to be seen whether this assay would carry the sensitivity to identify subtle differences in activation responses toward antigen-carrying EVs in specific demographics (e.g., age, sex, race, vaccine manufacturer) as the sample size used for validation in this study is not large enough to test these correlations. Additionally, the preferential uptake of EVs in antigen-presenting cells was identified in three experimental replicates using PBMCs from a single donor. As such, donor-to-donor variability is not captured in this finding; however, these findings are consistent with pre-existing literature on EV uptake dynamics.[52–55] Secondly, the results presented in this study suggest that EVs were highly effective in antigen delivery as the magnitude of the T cell response was similar to that of the positive controls (Spike protein and Spike peptides) while delivering quantitatively less Spike protein as determined by ELISA (1.26 ng in EV treatment compared to 1 μg of Spike protein control). The authors use caution when making a claim regarding the efficiency of antigen delivery by EVs because the use of SARS-CoV-2 pseudovirus for comparison would be more suitable to address this question. Lastly, it would be of great interest to utilize this assay in applications beyond SARS-CoV-2 and therefore further investigation is required to explore the broader use for the assessment of EV immunogenicity in the context of other antigens.

STAR★METHODS

Detailed methods are provided in the online version of this paper and include the following:

- KEY RESOURCES TABLE
- RESOURCE AVAILABILITY
  - Lead contact
  - Materials availability
  - Data and code availability
- EXPERIMENTAL MODEL AND STUDY PARTICIPANT DETAILS
  - Cell lines
  - Primary cell culture
- METHOD DETAILS
  - Gene design and synthesis
  - SARS-CoV-2 spike lentivirus production
  - Cell culture and cell conditioned medium production
  - SARS-CoV-2 spike immunofluorescence and microscopy
  - SARS-CoV-2 spike flow cytometry
  - EV isolation
  - Nanoparticle tracking analysis of EVs
  - Transmission electron microscopy (TEM) analysis of spike EVs and immunogold labeling of SARS-CoV-2 spike protein
  - EV surface marker profiling of 37 antigens by MACSPlex Exosome kit
  - EV characterization by Western Blotting
  - SARS-CoV-2 spike Enzyme-linked Immunosorbent assay (ELISA)
  - SARS-CoV-2 spike: ACE2 binding assay
  - PBMC culture and EV treatment
  - T cell AIM assay by flow cytometry
  - Antigen-presenting cell activation assay by flow cytometry

- EV uptake assay
- QUANTIFICATION AND STATISTICAL ANALYSIS

SUPPLEMENTAL INFORMATION

Supplemental information can be found online at https://doi.org/10.1016/j.isci.2023.108708.

ACKNOWLEDGMENTS

The authors would like to thank the Nanomedicines laboratory at the Center for Oncology, Radiopharmaceuticals and Research at Health Canada for their assistance with Nanoparticle Tracking Analysis measurements. The authors would also like to thank Jianqun Wang for the assistance with transmission electron microscopy at the Carleton University Nano Imaging Facility. The authors would like to thank Michael J. W. Johnston, Huixin Lu and Simon Sauve for their critical review of the article. Additionally, the authors would like to acknowledge that the graphical abstract was created with BioRender.com.

This work was supported by an operating grant from Genomics Research and Development Initiative (GRDI) Phase VII (2019–2024) obtained from the Government of Canada by JRL.

AUTHOR CONTRIBUTIONS

Conceptualization: SEC, SPD, TEG, TA, and JRL; data curation: SEC; formal analysis: SEC, SPD, and JRL; investigation: SEC, SPD, FSDB, AS, GM, JM, TEG, and TA; methodology: SEC, SPD, TEG, TA, and JRL; project administration: SEC, SPD, and JRL; visualization: SEC; writing – original draft: SEC and JRL; writing – review and editing: SPD, FSDB, AS, GM, JM, TEG, and TA; funding acquisition: JRL; supervision: JRL; resources: JRL.

DECLARATION OF INTERESTS

The authors declare that they have no competing interests.

Received: January 13, 2023
Revised: October 16, 2023
Accepted: December 8, 2023
Published: December 12, 2023

REFERENCES

1. Simons, M., and Raposo, G. (2009). Exosomes–vesicular carriers for intercellular communication. Curr. Opin. Cell Biol. *21*, 575–581.
2. van Niel, G., D'Angelo, G., and Raposo, G. (2018). Shedding light on the cell biology of extracellular vesicles. Nat. Rev. Mol. Cell Biol. *19*, 213–228.
3. Valadi, H., Ekström, K., Bossios, A., Sjöstrand, M., Lee, J.J., and Lötvall, J.O. (2007). Exosome-mediated transfer of mRNAs and microRNAs is a novel mechanism of genetic exchange between cells. Nat. Cell Biol. *9*, 654–659.
4. Mathieu, M., Martin-Jaular, L., Lavieu, G., and Théry, C. (2019). Specificities of secretion and uptake of exosomes and other extracelluar vesicles for cell-to-cell communication. Nat. Cell Biol. *21*, 9–17.
5. Mathivanan, S., Fahner, C.J., Reid, G.E., and Simpson, R.J. (2012). ExoCarta 2012: database of exosomal proteins, RNA and lipids. Nucleic Acids Res. *40*, D1241–D1244.
6. Théry, C., Witwer, K.W., Aikawa, E., Alcaraz, M.J., Anderson, J.D., Andriantsitohaina, R., Antoniou, A., Arab, T., Archer, F., Atkin-Smith, G.K., et al. (2018). Minimal information for studies of extracellular vesicles 2018 (MISEV2018): a position statement of the International Society for Extracellular Vesicles and update of the MISEV2014 guidelines. J. Extracell. Vesicles *7*, 1535750.
7. Zhang, Y., Liu, Y., Liu, H., and Tang, W.H. (2019). Exosomes: biogenesis, biologic function and clinical potential. Cell Biosci. *9*, 19.
8. Banks, W.A., Sharma, P., Bullock, K.M., Hansen, K.M., Ludwig, N., and Whiteside, T.L. (2020). Transport of Extracellular Vesicles across the Blood-Brain Barrier: Brain Pharmacokinetics and Effects of Inflammation. Int. J. Mol. Sci. *21*, 4407.
9. Morad, G., Carman, C.V., Hagedorn, E.J., Perlin, J.R., Zon, L.I., Mustafaoglu, N., Park, T.E., Ingber, D.E., Daisy, C.C., and Moses, M.A. (2019). Tumor-Derived Extracellular Vesicles Breach the Intact Blood-Brain Barrier via Transcytosis. ACS Nano *13*, 13853–13865.
10. Chang, C.L., Chen, H.H., Chen, K.H., Chiang, J.Y., Li, Y.C., Lin, H.S., Sung, P.H., and Yip, H.K. (2019). Adipose-derived mesenchymal stem cell-derived exosomes markedly protected the brain against sepsis syndrome induced injury in rat. Am. J. Transl. Res. *11*, 3955–3971.
11. Wang, X., Liu, D., Zhang, X., Yang, L., Xia, Z., and Zhang, Q. (2022). Exosomes from adipose-derived mesenchymal stem cells alleviate sepsis-induced lung injury in mice by inhibiting the secretion of IL-27 in macrophages. Cell Death Dis. *8*, 18.
12. Mao, F., Wu, Y., Tang, X., Kang, J., Zhang, B., Yan, Y., Qian, H., Zhang, X., and Xu, W. (2017). Exosomes Derived from Human Umbilical Cord Mesenchymal Stem Cells Relieve Inflammatory Bowel Disease in Mice. BioMed Res. Int. *2017*, 5356760.
13. Lai, P., Chen, X., Guo, L., Wang, Y., Liu, X., Liu, Y., Zhou, T., Huang, T., Geng, S., Luo, C., et al. (2018). A potent immunomodulatory role of exosomes derived from mesenchymal stromal cells in preventing cGVHD. J. Hematol. Oncol. *11*, 135.
14. Kordelas, L., Rebmann, V., Ludwig, A.K., Radtke, S., Ruesing, J., Doeppner, T.R., Epple, M., Horn, P.A., Beelen, D.W., and Giebel, B. (2014). MSC-derived exosomes: a novel tool to treat therapy-refractory graft-versus-host disease. Leukemia *28*, 970–973.
15. Fujii, S., Miura, Y., Fujishiro, A., Shindo, T., Shimazu, Y., Hirai, H., Tahara, H., Takaori-Kondo, A., Ichinohe, T., and Maekawa, T. (2018). Graft-Versus-Host Disease Amelioration by Human Bone Marrow Mesenchymal Stromal/Stem Cell-Derived Extracellular Vesicles Is Associated with Peripheral Preservation of Naive T Cell Populations. Stem Cell. *36*, 434–445.
16. Viaud, S., Théry, C., Ploix, S., Tursz, T., Lapierre, V., Lantz, O., Zitvogel, L., and Chaput, N. (2010). Dendritic cell-derived exosomes for cancer immunotherapy: what's next? Cancer Res. *70*, 1281–1285.
17. Wang, L., Xie, Y., Ahmed, K.A., Ahmed, S., Sami, A., Chibbar, R., Xu, Q., Kane, S.E., Hao, S., Mulligan, S.J., and Xiang, J. (2013). Exosomal pMHC-I complex targets T cell-based vaccine to directly stimulate CTL responses leading to antitumor immunity in transgenic FVBneuN and HLA-A2/HER2 mice and eradicating trastuzumab-resistant tumor

in athymic nude mice. Breast Cancer Res. Treat. *140*, 273–284.
18. Bu, N., Wu, H., Zhang, G., Zhan, S., Zhang, R., Sun, H., Du, Y., Yao, L., and Wang, H. (2015). Exosomes from Dendritic Cells Loaded with Chaperone-Rich Cell Lysates Elicit a Potent T Cell Immune Response Against Intracranial Glioma in Mice. J. Mol. Neurosci. *56*, 631–643.
19. Xiong, X., Ke, X., Wang, L., Lin, Y., Wang, S., Yao, Z., Li, K., Luo, Y., Liu, F., Pan, Y., et al. (2022). Neoantigen-based cancer vaccination using chimeric RNA-loaded dendritic cell-derived extracellular vesicles. J. Extracell. Vesicles *11*, e12243.
20. Besse, B., Charrier, M., Lapierre, V., Dansin, E., Lantz, O., Planchard, D., Le Chevalier, T., Livartoski, A., Barlesi, F., Laplanche, A., et al. (2016). Dendritic cell-derived exosomes as maintenance immunotherapy after first line chemotherapy in NSCLC. OncoImmunology *5*, e1071008.
21. Krishnan, A., Muthusamy, S., Fernandez, F.B., and Kasoju, N. (2022). Mesenchymal Stem Cell-Derived Extracellular Vesicles in the Management of COVID19-Associated Lung Injury: A Review on Publications, Clinical Trials and Patent Landscape. Tissue Eng. Regen. Med. *19*, 659–673.
22. Sengupta, V., Sengupta, S., Lazo, A., Woods, P., Nolan, A., and Bremer, N. (2020). Exosomes Derived from Bone Marrow Mesenchymal Stem Cells as Treatment for Severe COVID-19. Stem Cell. Dev. *29*, 747–754.
23. Wu, C., Xu, Q., Wang, H., Tu, B., Zeng, J., Zhao, P., Shi, M., Qiu, H., and Huang, Y. (2022). Neutralization of SARS-CoV-2 pseudovirus using ACE2-engineered extracellular vesicles. Acta Pharm. Sin. B *12*, 1523–1533.
24. Cocozza, F., Névo, N., Piovesana, E., Lahaye, X., Buchrieser, J., Schwartz, O., Manel, N., Tkach, M., Théry, C., and Martin-Jaular, L. (2020). Extracellular vesicles containing ACE2 efficiently prevent infection by SARS-CoV-2 Spike protein-containing virus. J. Extracell. Vesicles *10*, e12050.
25. Tanaka, S., Nelson, G., Olson, C.A., Buzko, O., Higashide, W., Shin, A., Gonzalez, M., Taft, J., Patel, R., Buta, S., et al. (2021). An ACE2 Triple Decoy that neutralizes SARS-CoV-2 shows enhanced affinity for virus variants. Sci. Rep. *11*, 12740.
26. Kim, H.K., Cho, J., Kim, E., Kim, J., Yang, J.S., Kim, K.C., Lee, J.Y., Shin, Y., Palomera, L.F., Park, J., et al. (2022). Engineered small extracellular vesicles displaying ACE2 variants on the surface protect against SARS-CoV-2 infection. J. Extracell. Vesicles *11*, e12179.
27. Lim, K., Nishide, G., Yoshida, T., Watanabe-Nakayama, T., Kobayashi, A., Hazawa, M., Hanayama, R., Ando, T., and Wong, R.W. (2021). Millisecond dynamic of SARS-CoV-2 spike and its interaction with ACE2 receptor and small extracellular vesicles. J. Extracell. Vesicles *10*, e12170.
28. Lim, K., Nishide, G., Sajidah, E.S., Yamano, T., Qiu, Y., Yoshida, T., Kobayashi, A., Hazawa, M., Ando, T., Hanayama, R., and Wong, R.W. (2023). Nanoscopic Assessment of Anti-SARS-CoV-2 Spike Neutralizing Antibody Using High-Speed AFM. Nano Lett. *23*, 619–628.
29. Tsai, S.J., Atai, N.A., Cacciottolo, M., Nice, J., Salehi, A., Guo, C., Sedgwick, A., Kanagavelu, S., and Gould, S.J. (2021). Exosome-mediated mRNA delivery in vivo is safe and can be used to induce SARS-CoV-2 immunity. J. Biol. Chem. *297*, 101266.
30. Jiang, L., Driedonks, T.A.P., Jong, W.S.P., Dhakal, S., Bart van den Berg van Saparoea, H., Sitaras, I., Zhou, R., Caputo, C., Littlefield, K., Lowman, M., et al. (2022). A bacterial extracellular vesicle-based intranasal vaccine against SARS-CoV-2 protects against disease and elicits neutralizing antibodies to wild-type and Delta variants. J. Extracell. Vesicles *11*, e12192.
31. Wang, Z., Popowski, K.D., Zhu, D., de Juan Abad, B.L., Wang, X., Liu, M., Lutz, H., De Naeyer, N., DeMarco, C.T., Denny, T.N., et al. (2022). Exosomes decorated with a recombinant SARS-CoV-2 receptor-binding domain as an inhalable COVID-19 vaccine. Nat. Biomed. Eng. *6*, 791–805.
32. Shen, A.-R., Jin, X.-X., Tang, T.-T., Ding, Y., Liu, X.-T., Zhong, X., Wu, Y.-D., Han, X.-L., Zhao, G.-Y., Shen, C.-L., et al. (2022). Exosomal Vaccine Loading T Cell Epitope Peptides of SARS-CoV-2 Induces Robust CD8+ T Cell Response in HLA-A Transgenic Mice. Int. J. Nanomed. *17*, 3325–3341.
33. Barnwal, A., Basu, B., Tripathi, A., Soni, N., Mishra, D., Banerjee, A., Kumar, R., Vrati, S., and Bhattacharyya, J. (2022). SARS-CoV-2 Spike Protein-Activated Dendritic Cell-Derived Extracellular Vesicles Induce Antiviral Immunity in Mice. ACS Biomater. Sci. Eng. *8*, 5338–5348.
34. Bansal, S., Perincheri, S., Fleming, T., Poulson, C., Tiffany, B., Bremner, R.M., and Mohanakumar, T. (2021). Cutting Edge: Circulating Exosomes with COVID Spike Protein Are Induced by BNT162b2 (Pfizer-BioNTech) Vaccination prior to Development of Antibodies: A Novel Mechanism for Immune Activation by mRNA Vaccines. J. Immunol. *207*, 2405–2410.
35. Anticoli, S., Manfredi, F., Chiozzini, C., Arenaccio, C., Olivetta, E., Ferrantelli, F., Capocefalo, A., Falcone, E., Ruggieri, A., and Federico, M. (2018). An Exosome-Based Vaccine Platform Imparts Cytotoxic T Lymphocyte Immunity Against Viral Antigens. Biotechnol. J. *13*, e1700443.
36. Hong, S., Ruan, S., Greenberg, Z., He, M., and McGill, J.L. (2021). Development of surface engineered antigenic exosomes as vaccines for respiratory syncytial virus. Sci. Rep. *11*, 21358.
37. Chiozzini, C., Manfredi, F., Arenaccio, C., Ferrantelli, F., Leone, P., and Federico, M. (2020). N-Terminal Fatty Acids of NEF(MUT) Are Required for the CD8(+) T-Cell Immunogenicity of In Vivo Engineered Extracellular Vesicles. Vaccines (Basel) *8*, 243.
38. Mestas, J., and Hughes, C.C.W. (2004). Of mice and not men: differences between mouse and human immunology. J. Immunol. *172*, 2731–2738.
39. Lan, J., Ge, J., Yu, J., Shan, S., Zhou, H., Fan, S., Zhang, Q., Shi, X., Wang, Q., Zhang, L., and Wang, X. (2020). Structure of the SARS-CoV-2 spike receptor-binding domain bound to the ACE2 receptor. Nature *581*, 215–220.
40. Yang, J., Petitjean, S.J.L., Koehler, M., Zhang, Q., Dumitru, A.C., Chen, W., Derclaye, S., Vincent, S.P., Soumillion, P., and Alsteens, D. (2020). Molecular interaction and inhibition of SARS-CoV-2 binding to the ACE2 receptor. Nat. Commun. *11*, 4541.
41. Tarke, A., Coelho, C.H., Zhang, Z., Dan, J.M., Yu, E.D., Methot, N., Bloom, N.I., Goodwin, B., Phillips, E., Mallal, S., et al. (2022). SARS-CoV-2 vaccination induces immunological T cell memory able to cross-recognize variants from Alpha to Omicron. Cell *185*, 847–859.e11.
42. Tarke, A., Sidney, J., Methot, N., Yu, E.D., Zhang, Y., Dan, J.M., Goodwin, B., Rubiro, P., Sutherland, A., Wang, E., et al. (2021). Impact of SARS-CoV-2 variants on the total CD4(+) and CD8(+) T cell reactivity in infected or vaccinated individuals. Cell Rep. Med. *2*, 100355.
43. Keeton, R., Tincho, M.B., Ngomti, A., Baguma, R., Benede, N., Suzuki, A., Khan, K., Cele, S., Bernstein, M., Karim, F., et al. (2022). T cell responses to SARS-CoV-2 spike cross-recognize Omicron. Nature *603*, 488–492.
44. Kuate, S., Cinatl, J., Doerr, H.W., and Uberla, K. (2007). Exosomal vaccines containing the S protein of the SARS coronavirus induce high levels of neutralizing antibodies. Virology *362*, 26–37.
45. Huddleston, C.A., Weinberg, A.D., and Parker, D.C. (2006). OX40 (CD134) engagement drives differentiation of CD4+ T cells to effector cells. Eur. J. Immunol. *36*, 1093–1103.
46. Taraban, V.Y., Rowley, T.F., O'Brien, L., Chan, H.T.C., Haswell, L.E., Green, M.H.A., Tutt, A.L., Glennie, M.J., and Al-Shamkhani, A. (2002). Expression and costimulatory effects of the TNF receptor superfamily members CD134 (OX40) and CD137 (4-1BB), and their role in the generation of anti-tumor immune responses. Eur. J. Immunol. *32*, 3617–3627.
47. Munks, M.W., Mourich, D.V., Mittler, R.S., Weinberg, A.D., and Hill, A.B. (2004). 4-1BB and OX40 stimulation enhance CD8 and CD4 T-cell responses to a DNA prime, poxvirus boost vaccine. Immunology *112*, 559–566.
48. Mendel, I., and Shevach, E.M. (2006). Activated T cells express the OX40 ligand: requirements for induction and costimulatory function. Immunology *117*, 196–204.
49. Kwon, B.S., Hurtado, J.C., Lee, Z.H., Kwack, K.B., Seo, S.K., Choi, B.K., Koller, B.H., Wolisi, G., Broxmeyer, H.E., and Vinay, D.S. (2002). Immune responses in 4-1BB (CD137)-deficient mice. J. Immunol. *168*, 5483–5490.
50. Grifoni, A., Weiskopf, D., Ramirez, S.I., Mateus, J., Dan, J.M., Moderbacher, C.R., Rawlings, S.A., Sutherland, A., Premkumar, L., Jadi, R.S., et al. (2020). Targets of T Cell Responses to SARS-CoV-2 Coronavirus in Humans with COVID-19 Disease and Unexposed Individuals. Cell *181*, 1489–1501.e15.
51. Mulcahy, L.A., Pink, R.C., and Carter, D.R.F. (2014). Routes and mechanisms of extracellular vesicle uptake. J. Extracell. Vesicles *3*.
52. Feng, D., Zhao, W.L., Ye, Y.Y., Bai, X.C., Liu, R.Q., Chang, L.F., Zhou, Q., and Sui, S.F. (2010). Cellular internalization of exosomes occurs through phagocytosis. Traffic *11*, 675–687.
53. Wiklander, O.P.B., Nordin, J.Z., O'Loughlin, A., Gustafsson, Y., Corso, G., Mäger, I., Vader, P., Lee, Y., Sork, H., Seow, Y., et al. (2015). Extracellular vesicle in vivo biodistribution is determined by cell source, route of administration and targeting. J. Extracell. Vesicles *4*, 26316.
54. Khare, D., Or, R., Resnick, I., Barkatz, C., Almogi-Hazan, O., and Avni, B. (2018). Mesenchymal Stromal Cell-Derived Exosomes Affect mRNA Expression and Function of B-Lymphocytes. Front. Immunol. *9*, 3053.
55. Di Trapani, M., Bassi, G., Midolo, M., Gatti, A., Kamga, P.T., Cassaro, A., Carusone, R., Adamo, A., and Krampera, M. (2016).

Differential and transferable modulatory effects of mesenchymal stromal cell-derived extracellular vesicles on T, B and NK cell functions. Sci. Rep. *6*, 24120.

56. Gurung, S., Perocheau, D., Touramanidou, L., and Baruteau, J. (2021). The exosome journey: from biogenesis to uptake and intracellular signalling. Cell Commun. Signal. *19*, 47.
57. Izquierdo-Useros, N., Naranjo-Gómez, M., Archer, J., Hatch, S.C., Erkizia, I., Blanco, J., Borràs, F.E., Puertas, M.C., Connor, J.H., Fernández-Figueras, M.T., et al. (2009). Capture and transfer of HIV-1 particles by mature dendritic cells converges with the exosome-dissemination pathway. Blood *113*, 2732–2741.
58. Pufnock, J.S., Cigal, M., Rolczynski, L.S., Andersen-Nissen, E., Wolfl, M., McElrath, M.J., and Greenberg, P.D. (2011). Priming CD8+ T cells with dendritic cells matured using TLR4 and TLR7/8 ligands together enhances generation of CD8+ T cells retaining CD28. Blood *117*, 6542–6551.
59. Schweitzer, A.N., and Sharpe, A.H. (1998). Studies using antigen-presenting cells lacking expression of both B7-1 (CD80) and B7-2 (CD86) show distinct requirements for B7 molecules during priming versus restimulation of Th2 but not Th1 cytokine production. J. Immunol. *161*, 2762–2771.
60. van Rijt, L.S., Vos, N., Willart, M., Kleinjan, A., Coyle, A.J., Hoogsteden, H.C., and Lambrecht, B.N. (2004). Essential role of dendritic cell CD80/CD86 costimulation in the induction, but not reactivation, of TH2 effector responses in a mouse model of asthma. J. Allergy Clin. Immunol. *114*, 166–173.
61. London, C.A., Lodge, M.P., and Abbas, A.K. (2000). Functional responses and costimulator dependence of memory CD4+ T cells. J. Immunol. *164*, 265–272.
62. Bowyer, G., Rampling, T., Powlson, J., Morter, R., Wright, D., Hill, A.V.S., and Ewer, K.J. (2018). Activation-induced Markers Detect Vaccine-Specific CD4(+) T Cell Responses Not Measured by Assays Conventionally Used in Clinical Trials. Vaccines (Basel) *6*.
63. Mateus, J., Dan, J.M., Zhang, Z., Rydyznski Moderbacher, C., Lammers, M., Goodwin, B., Sette, A., Crotty, S., and Weiskopf, D. (2021). Low-dose mRNA-1273 COVID-19 vaccine generates durable memory enhanced by cross-reactive T cells. Science *374*, eabj9853.
64. Dan, J.M., Lindestam Arlehamn, C.S., Weiskopf, D., da Silva Antunes, R., Havenar-Daughton, C., Reiss, S.M., Brigger, M., Bothwell, M., Sette, A., and Crotty, S. (2016). A Cytokine-Independent Approach To Identify Antigen-Specific Human Germinal Center T Follicular Helper Cells and Rare Antigen-Specific CD4+ T Cells in Blood. J. Immunol. *197*, 983–993.
65. Stothard, P. (2000). The Sequence Manipulation Suite: JavaScript Programs for Analyzing and Formatting Protein and DNA Sequences. Biotechniques *28*, 1102–1104.
66. Wrapp, D., Wang, N., Corbett, K.S., Goldsmith, J.A., Hsieh, C.-L., Abiona, O., Graham, B.S., and McLellan, J.S. (2020). Cryo-EM Structure of the 2019-nCoV Spike in the Prefusion Conformation. Science *367*, 1260–1263.
67. Muhle-Goll, C., Hoffmann, S., Afonin, S., Grage, S.L., Polyansky, A.A., Windisch, D., Zeitler, M., Bürck, J., and Ulrich, A.S. (2012). Hydrophobic matching controls the tilt and stability of the dimeric platelet-derived growth factor receptor (PDGFR) beta transmembrane segment. J. Biol. Chem. *287*, 26178–26186.
68. Gobin, J., Muradia, G., Mehic, J., Westwood, C., Couvrette, L., Stalker, A., Bigelow, S., Luebbert, C.C., Bissonnette, F.S.D., Johnston, M.J.W., et al. (2021). Hollow-fiber bioreactor production of extracellular vesicles from human bone marrow mesenchymal stromal cells yields nanovesicles that mirrors the immuno-modulatory antigenic signature of the producer cell. Stem Cell Res. Ther. *12*, 127.

STAR★METHODS

KEY RESOURCES TABLE

REAGENT or RESOURCE	SOURCE	IDENTIFIER
Antibodies		
SARS-CoV-2 Spike Protein (RBD) Chimeric Recombinant Rabbit Monoclonal Antibody (T01KHuRb)	Invitrogen	Cat#703959; RRID: AB_2866478
Alexa Fluor 488 Goat anti-Rabbit IgG Secondary	Invitrogen	Cat#A11034; RRID: AB_2576217
Gold (10 nm) IgG Donkey anti-Rabbit	Abcam	Cat#ab39597; RRID: AB_954430
SARS-CoV-2 Spike Protein (S1-NTD), Rabbit	Cell Signaling Tech	Cat#56996
Calnexin Antibody, Rabbit	Cell Signaling Tech	Cat#2433; RRID: AB_2243887
GM130 Antibody, Mouse, Clone 35	BD Transduction Laboratories	Cat#610822; RRID: AB_398142
Mouse Anti-Human CD63, Clone H5C6	BD Biosciences	Cat#556019; RRID: AB_396297
Rabbit Anti-Human CD9, Clone EPR23105-121	Abcam	Cat#ab236630; RRID: AB_2922400
Mouse Anti-Flotillin-1, Clone 18	BD Transduction Laboratories	Cat#610820; RRID: AB_398139
GAPDH Antibody [GT239], Mouse	GeneTex	Cat#GTX627408; RRID: AB_11174761
TSG101 Antibody [4A10], Mouse	Novus Biologicals	Cat#NB200-112; RRID: AB_2256458
Anti-CD3-AF700, Clone SP34-2	BD Pharmingen	Cat#557917; RRID: AB_396938
Anti-CD4-APC, Clone RPA-T4	BD Pharmingen	Cat#555349; RRID: AB_398593
Anti-CD8-BV421, Clone RPA-T8	BD Horizon	Cat#562428; RRID: AB_11154035
Anti-CD69-BV650, Clone FN50	BD Horizon	Cat#563835; RRID: AB_2738442
Anti-CD134-PE/Cy7, Clone ACT35	Biolegend	Cat#350012; RRID: AB_10901161
Anti-CD137-PE/Cy5, Clone 4B4-1	Biolegend	Cat#309808; RRID: AB_830670
Anti-CD19-BUV737, Clone SJ25C1	BD Horizon	Cat#612756; RRID: AB_2870087
Anti-CD14-BV510, Clone M5E2	BD OptiBuild	Cat#740163; RRID: AB_2739916
Anti-CD16-BV711, Clone 3G8	Biolegend	Cat#302044; RRID: AB_2563802
Anti-CD80-BV421, Clone L307.4	BD Horizon	Cat#564160; RRID: AB_2738632
Anti-CD86-APC, Clone BU63	Biolegend	Cat#374208; RRID: AB_2721449
Anti-HLA-DR-PE, Clone G46-6	BD Pharmingen	Cat#555812; RRID: AB_396146
Biological samples		
Human Peripheral Blood Mononuclear Cells	RayBiotech Inc	Cat#CoV-PBMC-V-10
Chemicals, peptides, and recombinant proteins		
LV-MAX Transfection Kit	Gibco	Cat#A35346
Second Generation Packaging System Mix	abm	Cat#LV003
LV-MAX Production Medium	Gibco	Cat#A3583401
FreeStyle 293 Expression Medium	ThermoFisher	Cat#12338018
Blasticidin	Invivogen	Cat#ant-bl-05
D-PBS	Gibco	Cat#14190250
Goat Serum	Sigma	Cat#S26-100ML
IgG-Free Bovine Serum Albumin	Sigma	Cat#A0336-50mL
Propidium Iodide	Invitrogen	Cat#P1304MP
Fetal Bovine Serum	Gibco	Cat#12483-020

(*Continued on next page*)

Continued

REAGENT or RESOURCE	SOURCE	IDENTIFIER
Paraformaldehyde	Electron Microscopy Sciences	Cat#15710
5X RIPA Buffer	Alfa Aesar	Cat#J62524-AE
HALT Protease and Phosphatase Inhibitors	ThermoFisher	Cat#78441
1X RIPA Buffer	Pierce	Cat#PI8990
4X LI-COR Protein Loading Buffer	LI-COR	Cat#928-40004
Bolt 10X Sample Reducing Agent	Invitrogen	Cat#B0009
Bolt 4–12% Bis-Tris Plus gels	Invitrogen	Cat#NW04122BOX
Immobilon FL PVDF membrane	Millipore	Cat#IPFL00005
iBind Solution	Invitrogen	Cat#SLF2019
IRDye 800CW Goat anti-Mouse	LI-COR	Cat#925-32210
IRDye 800CW Goat anti-Rabbit	LI-COR	Cat#925-32211
ImmunoCult-XF T cell Expansion Medium	StemCell Technologies	Cat#10981
PepTivator SARS-CoV-2 Prot_S	Miltenyi Biotech	Cat#130-126-700
Recombinant SARS-CoV-2 Spike Protein	R&D Systems	Cat#10549-CV
Carboxyfluoresceine diacetate succinimidyl-ester	Life Technologies	Cat#C34554
Critical commercial assays		
MACSplex Exosome Kit (human)	Miltenyi Biotec	Cat#130-108-813
Pierce BCA Protein Assay Kit	ThermoFisher	Cat#23227
COVID-19 S-Protein (S1RBD) ELISA Kit	RayBiotech Inc	Cat#ELV-COVID19S1-1
Spike-ACE2 Binding Assay	RayBiotech Inc	Cat#CoV-SACE2-1
Experimental models: Cell lines		
HEK 293F Viral Production Cells	Gibco	Cat#A35347
Freestyle 293F Cells	ThermoFisher	Cat#R79007
Recombinant DNA		
pCDH-EF1s lentiviral plasmid	Kazuhiro Oka	Addgene: 72484; RRID: Addgene_72484
pCDH-EF1s-Spikemod	This paper	N/A
Software and algorithms		
Sequence Manipulator Suite	Stothard (2000)[65]	N/A
Zen 2	Zeiss	N/A
FACSDiva v9.0.2	BD Biosciences	N/A
FlowJo v10.8.1	FlowJo LLC	N/A
NTA 3.0	Malvern Instruments	N/A
GraphPad Prism v7	GraphPad Software	N/A
Other		
HiScreen CaptoCore 700 Size Exclusion Column	Cytvia	Cat#17548115
Amicon Ultra 15 centrifugal tubes (MWCO 10 kDa)	Millipore	Cat#UFC901024
Vivaspin 300 kDa filter	Sartorius	Cat#VS0651
Formvar-Carbon Coated Electron Microscopy Grids	Electron Microscopy Sciences	Cat#FCF300-CU
Zeba spin desalting columns (7K MWCO, 2 mL)	ThermoFisher	Cat#89890

RESOURCE AVAILABILITY

Lead contact

Further information and requests for resources and reagents should be directed to and will be fulfilled by the lead contact, Jessie R. Lavoie (jessie.lavoie@hc-sc.gc.ca).

Materials availability

New unique materials generated in this study are available upon request.

Data and code availability

- All data reported in this paper will be shared by the lead contact upon request.
- This paper does not report original code.
- Any additional information required to reanalyze the data reported in this paper is available from the lead contact upon request.

EXPERIMENTAL MODEL AND STUDY PARTICIPANT DETAILS

Cell lines

HEK 293F viral production cells (Gibco, A35347) were commercially obtained and used for production of lentivirus. Cells were maintained in LV-MAX Production Medium (Gibco, A3583401) in shaker flasks shaking at 135 RPM in a 37°C incubator at 8% CO_2. Cells were subcultured every 2–3 days as per recommendation by the supplier. HEK 293F viral production cells were not authenticated in house. HEK 293F viral production cells were tested and confirmed negative for mycoplasma contamination.

FreeStyle 293F cells (ThermoFisher, R79007) were commercially obtained. Cells were maintained in FreeStyle 293 Expression Medium (ThermoFisher, 12338018) in shaker flasks shaking at 135 RPM in a 37°C incubator at 8% CO_2. Cells were subcultured every 2–3 days as per recommendation by the supplier. FreeStyle 293F cells were not authenticated in house. FreeStyle 293F cells were tested and confirmed negative for mycoplasma contamination.

Primary cell culture

Frozen human PBMCs were provided by a commercial vendor (RayBiotech Inc, CoV-PBMC-V-10; Stem Cell Technologies). All PBMC samples were allocated into two experimental groups based on vaccination status: vaccinated donors and unvaccinated donors. All vaccinated donors (N = 9) had received two doses of an mRNA-based vaccine against SARS-CoV-2, either mRNA-1273 (Moderna) or BNT162b2 (Pfizer). Blood was collected from donors within 35 days of second vaccine. All unvaccinated samples (N = 3) are identified as individuals with blood collected prior to vaccination, or prior to the availability of a vaccine. Additional donor characteristics are summarized in Table S1. Ethics approval for experiments involving human-derived PBMC samples was obtained from the Health Canada-Public Health Agency of Canada Research Ethics Board under protocol number REB 2019-022H. PBMCs were thawed and maintained in culture in ImmunoCult-XF T cell Expansion Medium (StemCell Technologies; 10981) in 96 well round-bottom plates at a cell density of 1.0×10^5 or 2.0×10^5 PBMCs per well (experiment dependent) in a 37°C, 5% CO_2 incubator.

METHOD DETAILS

Gene design and synthesis

The stabilized SARS-CoV-2 Spike peptide sequence was used as described by Wrapp et al.[66] PDGFRbeta transmembrane domain sequence was used as listed by Muhle-Goll et al.[67] Peptide sequences were reverse translated and codon optimized using the Reverse Translate tool of Sequence Manipulation Suite.[65] Transgenes were synthesized by BioBasic (Toronto, Canada). The SARS-CoV-2 Spike transgene was subcloned into a pCDH-EF1s lentiviral plasmid, a gift from Kazuhiro Oka (Addgene plasmid #72484; RRID:Addgene_72484) to generate a SARS-CoV-2 Spike lentiviral transfer vector. Plasmid map can be found in Figure S1A.

SARS-CoV-2 spike lentivirus production

Lentivirus (LV) was produced in HEK 293F viral production cells (Gibco, A35347) using the LV-MAX Transfection Kit (Gibco, A35346) exactly as recommended by the manufacturer using the 30 mL shaker flask culture specifications. Second generation packaging system mix (abm, LV003) was used along with the synthesized SARS-CoV-2 Spike LV transfer vector. Harvest and concentration of the produced LV was performed exactly as recommended by the manufacturer of the LV-MAX Transfection Kit.

Cell culture and cell conditioned medium production

Freestyle 293-F cells, herein referred to as 293F cells, (ThermoFisher, R79007) were allowed to recover from thawing for 5 passages before LV transduction. SARS-CoV-2 Spike LV was added to recovered 293F cells to generate "293F Spike" transduced cells. 24 h after LV delivery, 293F cells were spun at 250 x g for 10 min to remove residual LV and resuspended in FreeStyle 293 Expression Medium supplemented with 20 μg/mL blasticidin (Invivogen, ant-bl-05) for antibiotic selection. Selection dose of blasticidin was maintained for one additional passage of the cells. Following this passage, cells were spun at 250 x g for 10 min and resuspended in FreeStyle 293 Expression Medium supplemented with 1 μg/mL blasticidin for maintenance of the SARS-CoV-2 Spike expressing line. Non-transduced cells, "293F cells", were also maintained at the same passage frequencies as controls. Once the 293F Spike cell line was established, cell conditioned medium (CCM) from both 293F Spike cells and control 293F cells was collected at each cell passage (every 2–3 days). To collect CCM, cells were centrifuged first at 250 × g for 10 min to remove cells followed by a second centrifugation at 2000 × g for 30 min to remove debris. The cleared CCM was then frozen and stored at −80°C until ready for EV isolation.

SARS-CoV-2 spike immunofluorescence and microscopy

293F cells (transduced and control) were collected and washed with D-PBS (Gibco, 14190250). Cells were incubated with blocking buffer (10% goat serum, Sigma, S26-100 ML; 1% IgG free bovine serum albumin, Sigma, A0336-50 mL; D-PBS) for 1 h at room temperature. After incubation, blocking buffer was aspirated and cells were incubated for 1 h at room temperature with primary antibody against SARS-CoV-2 spike (1:200; Invitrogen, 703959) prepared in staining buffer (1% IgG free bovine serum albumin in D-PBS). After incubation, cells were washed three times with D-PBS followed by a 1 h incubation at room temperature in Alexa Fluor 488 Goat anti-Rabbit IgG secondary antibody (1:1000; Invitrogen, A11034). Cells were then washed twice with D-PBS. Following washes, cells were suspended in propidium iodide (Invitrogen, P1304MP) diluted 1:1000 in D-PBS as a cell viability dye. Following two washes in D-PBS cells were transferred to a 24-well plate for imaging. Immunofluorescent images were acquired using a Zeiss AxioObserver.Z1 microscope with an AxioCam 506 color camera and Zen 2 software.

SARS-CoV-2 spike flow cytometry

293F cells (transduced and control) were collected, washed with flow buffer (D-PBS +2% Fetal Bovine Serum (Gibco, 12483-020)), and filtered through a 40 μm cell strainer to remove aggregates. Cells were then incubated in flow buffer with SARS-CoV-2 spike primary antibody (0.24 μg per test; Invitrogen, 703959) diluted in flow buffer for 30 min on ice. Cells were then washed two times with flow buffer, after which they were incubated in secondary antibody (Alexa Fluor 488 Goat anti-Rabbit IgG secondary antibody; Invitrogen, A11034) diluted 1:2000 in flow buffer. Following two washes with flow buffer, cells were suspended in flow buffer supplemented with propidium iodide (1:2000; Life Technologies, P1304MP) for acquisition. Samples were acquired using a FACS Aria Fusion (BD Biosciences), FACSDiva (v9.0.2, BD Biosciences) software for acquisition and FlowJo (v10.8.1, FlowJo LLC) for analysis.

EV isolation

To isolate EVs from 293F to 293F Spike cells, frozen CCM was thawed overnight at 4°C and then centrifuged at 10,000xg for 60 min at 4°C to remove additional debris. The supernatant was collected and used for EV purification using fast protein liquid chromatography (FPLC; AKTA Start, Cytiva) outfitted with a size exclusion column (HiScreen CaptoCore 700; Cytvia, 17548115), as done previously.[68] For each purification, 40–60 mL of CCM was injected for SEC by FPLC. EV-containing fractions were collected once the UV readings reached their maximum plateau and fractionation was stopped once the UV readings began to fall. Following FPLC-mediated size exclusion, the samples were concentrated via ultrafiltration using Amicon Ultra 15 centrifugal tubes (MWCO 10 kDa, Millipore, UFC901024) and filtered using pre-wet 0.22 μM filters (Pall, 4612) for sterile use.

Nanoparticle tracking analysis of EVs

Once collected, EVs were analyzed by nanoparticle tracking analysis (NTA) using the NanoSight NS 3000 (Malvern Panalytical), as described previously with some modifications.[68] Concentrated EV samples were diluted in filtered-D-PBS (Gibco, 14190) and a final volume of 1 mL of diluted EV sample was used for analysis. Samples were analyzed in flow mode using a syringe pump (Harvard Apparatus, 98–4730). Each 1 mL sample was run such that 5 captures of 1 min per capture at a speed of 10 under flow mode were acquired. Between each capture, 0.1 mL of sample was injected to ensure varied sampling across the syringe. For capture settings, a camera level of 14 was used for all samples and a detection threshold of 11 was used for analysis resulting in approximately 25–35 particles per frame. Analysis of the raw data utilized the NTA 3.0 software (Malvern Instruments).

Transmission electron microscopy (TEM) analysis of spike EVs and immunogold labeling of SARS-CoV-2 spike protein

Purified Spike EVs (2×10^9) were added to a Vivaspin 300 kDa filter (Sartorius, VS0651) pre-equilibrated with filtered D-PBS and centrifuged at 2000xg for 3 min. The EVs were then suspended in 100 μL of 4% paraformaldehyde (PFA; Electron Microscopy Sciences, 15710), for collection and transferred into a low bind Eppendorf tube. The retentate component of the Vivaspin filter was washed with 100 μL of 4% PFA two more times and those volumes were transferred into the low bind Eppendorf tube as well for a resultant 300 μL fixed-EV solution. After a minimum of 30 min incubation, a 40 μL drop of fixed-EV solution was added to parafilm where a glow-discarded (45 s) formvar-carbon coated EM grids (Electron Microscopy Sciences; FCF300-CU) was added on top of the fixed-EV drop and rested for 10 min. Each grid was rinsed in four drops (1 min each) of 50 μL filtered D-PBS before processing for SARS-CoV-2 Spike protein immuno-gold labeling. For immuno-gold labeling, each grid was incubated for 1 h with a drop of 1:100 Rb-SARS-CoV-2 Spike Protein (T01KHuRb) antibody (Invitrogen, 703959). Each grid was rinsed into two drops (5 min each) of 50 μL filtered D-PBS before incubating each grid for 2 h with a drop of 1:20 Gold (10 nm) IgG Donkey anti-Rabbit (Abcam, ab39597). Each grid was rinsed into three drops (5 min each) of 50 μL filtered D-PBS. All grids were allowed to air dry for at least 30 min before imaging on the EI Tecnai G2 Spirit Twin TEM with a Lab6 emitter, operating at 120 kV, at Carleton Nano Imaging Facility, Canada. The images were acquired with an Eagle camera with a 16K resolution. All steps were performed at room temperature.

EV surface marker profiling of 37 antigens by MACSPlex Exosome kit

Multiplex bead-based, flow cytometric analysis of 37 surface antigens was conducted to characterize harvested EVs using the MACSplex Exosome kit (human; Miltenyi Biotec, 130-108-813). Samples were processed according to manufacturer's instructions using the "Overnight protocol for the assay using 1.5 mL tubes", with some modifications. Briefly, 460 μL of EV sample and 40 μL of MACSplex Exosome Capture Beads were combined in a 1.5-mL Protein LoBind tubes (Eppendorf, cat#0030.108.116) and incubated overnight in an orbital shaker set at 4°C and

450 RPM. Following execution of all labeling steps outlined in the manufacturer's protocol, samples were transferred to 5-mL FACS tubes (BD Biosciences, 382058) for analysis by flow cytometry using the FACSAria Fusion flow cytometer (BD Biosciences). Raw data was analyzed using FlowJo (V10.8.1, FlowJo LLC). For data analysis, background was subtracted first by including buffer only controls for each bead, and further through subtraction of isotype control signal.

EV characterization by Western Blotting

293F and 293F Spike EVs were lysed in 5X RIPA buffer (Alfa Aesar, J62524-AE) with the addition of 1X HALT protease and phosphatase inhibitors (Thermo Fisher Scientific, 78441) and transferred to a 1.5 mL Protein LoBind tube (Eppendorf, 0030.108.116). 239F and 293F Spike cells were centrifuged at 250 x g for 10 min to collect a cell pellet. Cell pellets were lysed in 1X RIPA buffer (Pierce, PI8990) with the addition of 1X HALT protease and phosphatase inhibitors and transferred to a 1.5 mL Protein LoBind tube. All samples were then put on an end-over-end shaker (LabQuake Shaker) and incubated for 30 min at 4°C. Following incubation, samples were sonicated on ice. The sonication settings used for EV lysates were: amplitude at 20% of maximum with 10 s pulse and 30 s rest on ice, repeated three times. The sonication settings used for cell lysates were: amplitude at 30% of maximum with 10 s pulse and 30 s rest on ice, repeated three times. All lysates were then centrifuged at 14,000xg for 5 min at 4°C. The supernatant was stored at −80°C until ready for processing. Protein content for all samples was determined by the Pierce BCA Protein Assay Kit (Thermo Fisher Scientific, 23227). For Western blot analysis, 20 µg of cell protein lysates and EV protein lysates were combined with 4X LI-COR Protein Loading Buffer (LI-COR, 928–40004) and Bolt 10X Sample Reducing Agent (Invitrogen, B0009) to a final concentration of 1X. For CD63 and CD9 detection, sample reducing agent was left out of sample preparation. Samples were boiled for 5 min and then loaded onto precast Bolt 4–12% Bis-Tris Plus gels (Invitrogen, NW04122BOX). Gels were run using a MOPS buffer system (Invitrogen, B0001) for 30 min at 200 V. Gels were trimmed and transferred to a Millipore Immobilon FL PVDF membrane (Millipore, IPFL00005) using the Bolt Mini Module wet transfer system for 1 h at 20V. Following transfer, membranes were dried. Membranes were then reactivated in methanol, rinsed in D-PBS for 5 min at room temperature and washed once in distilled water for 5 min on an orbital shaker at speed 4 (~300 RPM). Blots were stained with the Revert 700 Total Protein Stain Kit (LI-COR, 926–11010) according to the manufacturer's protocol and imaged at 700 nm using the LI-COR Odyssey CLx NIR imager (LI-COR Biosciences). For target detection, membranes were incubated in blocking buffer (iBind solution; Invitrogen, SLF2019) for 1 h at room temperature on an orbital shaker at approximately 300 RPM. Using the iBind Western Blot System (Invitrogen, SLF1000), membranes were probed with the following primary antibodies diluted in iBind solution (Invitrogen, SLF2019): anti-SARS-CoV-2 Spike (Cell Signaling Tech, 56996, 1:1000) anti-Calnexin (Cell Signaling Tech, 2433, 1:500), anti-GM130 (BD Transduction Laboratories, 610822, 1:500), anti-CD63 (BD Biosciences, 556019, 1:1000), anti-CD9 (Abcam, ab236630, 1:1000), anti-Flotillin-1 (BD Transduction Laboratories, 610820, 1:500), anti-GAPDH (GeneTex, GTX627408; 1:1000), and anti-TSG101 (Novus, NB200-112, 1:250) The following secondary antibodies were diluted 1:4000 in iBind solution: IRDye 800CW Goat anti-Mouse (LI-COR, 925–32210) and IRDye 800CW Goat anti-Rabbit (LI-COR, 925–32211) Following antibody incubation, membranes were rinsed in distilled water twice for 2 min and imaged. All image captures were performed at 800 nm using the LI-COR Odyssey CLx NIR imager. Full length gels can be found in Figure S4.

SARS-CoV-2 spike Enzyme-linked Immunosorbent assay (ELISA)

Lysates for three separate EV preparations were produced with 5X RIPA buffer exactly as was done in the "EV characterization by western blotting" section and were stored at −80°C until ready for processing. SARS-CoV-2 Spike protein levels were measured in these EV lysates using a COVID-19 S-Protein (S1RBD) ELISA Kit (Ray Biotech, ELV-COVID19S1-1). Manufacturer's instructions for this kit were followed exactly. For data analysis, readings taken at 540 nm were subtracted from 450 nm readings for wavelength correction. Data were then imported to GraphPad Prism version 7 (GraphPad Software) to interpolate concentrations based on the generation of a four-parameter logistic (4-PL) curve fit.

SARS-CoV-2 spike: ACE2 binding assay

Three separate preparations of EVs were performed for use in this assay and resultant EVs were first assessed by NTA to determine particle concentration in each sample. Based on the NTA results, 293F EVs and Spike EVs were diluted in appropriate volumes of D-PBS to generate four doses: 1×10^9, 2×10^9, 3×10^9 and 4×10^9 of EVs.

To assess SARS-CoV-2 Spike binding functionality on Spike EVs, a Spike-ACE2 binding assay kit was used (Ray Biotech, CoV-SACE2-1), following manufacturer's instructions with some modification. Briefly, this kit is formulated such that a plate coated with SARS-CoV-2 Spike protein is provided. 293F EVs or Spike EVs at the doses listed above were combined with the soluble ACE2 protein provided in the kit and then added to the plate and incubated for 2.5 h at room temperature with gentle shaking. The plate was then washed and incubated with a detection antibody directed toward the recombinant ACE2 protein. Following recommended incubation and washes, an HRP-conjugated detection antibody was added and allowed to incubate again with gentle shaking. Finally, after washes, the HRP signal was developed for 30 min using TMB One-Step Substrate reagent and, following addition of the stop solution, the plate was read at 450 nm. For data analysis, vehicle blank OD values were subtracted from sample OD values. The percent binding inhibition was then determined using the following calculation: % Binding Inhibition = [(OD of Maximum ACE2 signal)-(OD of sample)/(OD of Maximum ACE2 signal)] x 100.

PBMC culture and EV treatment

Frozen human PBMCs were thawed and maintained in culture in ImmunoCult-XF T cell Expansion Medium (StemCell Technologies; 10981) in 96 well round-bottom plates at a cell density of 2.0×10^5 PBMCs per well in a 37°C, 5% CO_2 incubator. PBMCs were allowed to recover for 24 h

in this media, at which time cells were treated with 293F or 293F Spike EVs at a concentration of 1.0×10^4 EV per PBMC. Treatments with SARS-CoV-2 peptides (PepTivator SARS-CoV-2 Prot_S; Miltenyi Biotech; 130-126-700) and recombinant SARS-CoV-2 Spike protein (with K986P, V987P, R682S and R685S mutations as well as C-term His tag; R&D Systems, 10549-CV) were included as positive controls. A treatment of 2 μL of SARS-CoV-2 peptide pool was used per 2.0×10^5 PBMCs, which is approximately 0.1 μg of each peptide per well (7 peptide species included in cocktail). A treatment of 1 μg of recombinant SARS-CoV-2 Spike protein was used per 2.0×10^5 PBMCs. PBMCs were collected 24 h (antigen-presenting cell activation) or 48 h (T cell activation induced marker [AIM] assay) following treatment for immediate processing for flow cytometry. Four wells of PBMCs were dedicated to each treatment group and were pooled together at the time of collection.

T cell AIM assay by flow cytometry

PBMCs were collected, washed with flow buffer (PBS +2% Fetal Bovine Serum (Gibco, 12483-020)), and filtered through a 40 μm cell strainer to remove aggregates. Cells were then incubated in flow buffer with the following anti-human antibodies: anti-CD3-AF700 (BD Pharmingen, 557917), anti-CD4-APC (BD Pharmingen, 555349), CD8-BV421 (BD Horizon, 562428), CD69-BV650 (BD Horizon, 563835), CD134-PE/Cy7 (Biolegend, 350012), CD137-PE/Cy5 (Biolegend, 309808) for 30 min on ice. Cells were washed with flow buffer and then suspended in flow buffer for acquisition. Propidium iodide (1:1000; Life Technologies, P1304MP) was added just before running. Samples were acquired using a FACS Aria Fusion (BD Biosciences) and a minimum of 500,000 events were captured per sample. FACSDiva (v9.0.2, BD Biosciences) software was used for acquisition and FlowJo (v10.8.1, FlowJo LLC) for analysis.

Antigen-presenting cell activation assay by flow cytometry

PBMCs were collected and washed with flow buffer (PBS +2% Fetal Bovine Serum (Gibco, 12483-020)). Cells were then incubated in flow buffer with the following anti-human antibodies: anti-CD3-AF700 (BD Pharmingen, 557917), anti-CD19-BUV737 (BD Horizon, 612756), anti-CD14-BV510 (BD OptiBuild, 740163), anti-CD16-BV711 (Biolegend, 302044), anti-CD80-BV421 (BD Horizon, 564160), anti-CD86-APC (Biolegend, 374208) and anti-HLA-DR-PE (BD Pharmingen, 555812) for 30 min on ice. Cells were washed with flow buffer and then suspended in flow buffer for acquisition. Propidium iodide (1:1000; Life Technologies, P1304MP) was added just before running. Samples were acquired using a FACS Aria Fusion (BD Biosciences) and a minimum of 500,000 events were captured per sample. FACSDiva (v9.0.2, BD Biosciences) software was used for acquisition and FlowJo (v10.8.1, FlowJo LLC) for analysis.

EV uptake assay

EV uptake assay: CFSE staining of EVs

Spike EVs were incubated with 250 μM of carboxyfluoresceine diacetate succinimidyl-ester (CFSE; Life Technologies, C34554) in 1.5-mL Protein LoBind tubes (Eppendorf, cat#0030.108.116) for 60 min with gentle mixing (450 RPM on orbital shaker). The same volume of D-PBS combined with 250 μM of CFSE was incubated alongside the EVs as a negative control for the assay. Zeba spin desalting columns (7K MWCO, 2 mL; ThermoFisher Scientific, 89890) were used to wash both Spike EVs + CFSE and PBS + CFSE samples following incubation to remove unbound CFSE. To do so, desalting columns were first prepared exactly as per manufacturer's instructions with 3 D-PBS washes. Once prepared, Spike EVs + CFSE and PBS + CFSE samples were removed from orbital shaker and transferred to the compact resin beds in separate desalting columns. Samples were then spun at 1500 x g for 2 min, as per manufacturer's recommendation. NTA analysis was performed on Spike EVs + CFSE sample exactly as outlined in "nanoparticle tracking analysis of EVs" to determine particle concentration for dosing.

EV uptake assay: PBMC treatment with CFSE-stained EVs

Frozen human PBMCs provided by a commercial vendor (RayBiotech Inc, CoV-PBMC-V-10) from a single donor (Donor 965) vaccinated against SARS-CoV-2 were thawed and maintained in culture in ImmunoCult-XF T cell Expansion Medium (StemCell Technologies; 10981) in 96 well round-bottom plates at a cell density of 1.0×10^5 PBMCs per well. PBMCs were allowed to recover for one day in this media, at which time cells were treated with PBS as a vehicle control, PBS + CFSE or Spike EV + CFSE, then returned to 37°C, 5% CO_2 incubator for approximately 16 h of incubation. PBMCs were collected following this incubation for immediate processing for flow cytometry. Five wells of PBMCs were dedicated to each treatment group and were pooled together at the time of processing. Three independent experimental replicates using the same PBMC donor were completed with three independent EV isolations.

EV uptake assay in PBMCs: Flow cytometry

PBMCs were collected, washed with flow buffer (PBS +2% Fetal Bovine Serum (Gibco, 12483-020)), and filtered through a 40 μm cell strainer to remove aggregates. Cells were then incubated in flow buffer with anti-human antibodies targeting the following: CD3-AF700 (BD Pharmingen, 557917), CD4-APC (BD Pharmingen, 555349), CD8-BV421 (BD Horizon, 562428), CD19-BUV737 (BD Horizon, 612756), CD14-BV510 (BD OptiBuild, 740163), CD16-BV711 (Biolegend, 302044), HLA-DR-PE (BD Pharmingen, 555812) for 30 min on ice. Cells were then washed with flow buffer, after which they were suspended in flow buffer supplemented with propidium iodide (1:1000; Life Technologies, P1304MP) and left to incubate for 10 min prior to acquisition. Samples were acquired using a FACS Aria Fusion (BD Biosciences) and a minimum of 400,000 events were captured per sample. FACSDiva (v9.0.2, BD Biosciences) software was used for acquisition and FlowJo (v10.8.1, FlowJo LLC) for analysis. Full gating strategy detailed in Figure S3. The t-SNE plugin in FlowJo was used for dimensionality reduction on data following preliminary gating which excluded dead cells and doublets. The flow cytometry data collected from PBS-treated, PBS and CFSE-treated and

Spike EV with CFSE-treated PBMCs from a single run were downsampled such that 50,000 events from each group were randomly selected. All cell phenotyping markers (CD3, CD4, CD8, CD19, CD14, CD16 and HLA-DR) were used for running the Barnes-Hut algorithm, was set to run 1000 iterations for the generation of the final t-SNE map. Manual gating of cell populations (Following the gating strategy in Figure S3) was overlayed onto t-SNE maps for each condition.

QUANTIFICATION AND STATISTICAL ANALYSIS

Statistical analyses were performed using GraphPad Prism version 7 (GraphPad Software). Specifications of statistical tests used and sample number can be found in the legend of each figure. In all statistical tests, p value <0.05 was considered statistically significant.